UNIVERSITAT POLITÈCNICA DE CATALUNYA

UNIVERSITAT DE BARCELONA

Projecte Final d'Estudis
MÀSTER
EN
ENGINYERIA BIOMÈDICA

EB

Quantification of surface dose during radiotherapy: Monte Carlo simulations and extrapolation chamber measurements.

Barcelona, May 2nd 2013.

Autor: Ingrid Isabel Valencia Lozano.
Director: Dra. María Amor Duch.

Realitzat a: INTE, Universitat Politècnica de Catalunya-
Hospital de la Santa Creu i Sant Pau.

" [...] humanity also needs dreamers, for whom the disinterested development of an enterprise is so captivating that it becomes impossible for them to devote their care to their own material profit. Without doubt, these dreamers do not deserve wealth, because they do not desire it. Even so, society should assure to such workers the efficient means of accomplishing their task, in a life freed from material care and freely consecrated to research."

Marie Sklodowska Curie

ABSTRACT

During a radiotherapy treatment, skin of the patient is always exposed to the radiation; as a consequence late effects can be appear. Therefore, dose values in this region may be of interest for clinical evaluation and investigation of those undesirable effects. However, surface dose is not intuitive and is difficult to measure and calculate; the parameters, which modify it are not always the same and each one are dependent to the others. The aim of this project is to quantify absorbed dose in the build-up region and near to the skin approximately between 0 mm - 1 mm using two methods. One of them, an analytical calculation using Monte Carlo simulations; and the other an experimental approach using an extrapolation chamber.

Monte Carlo simulations are performed with the PENELOPE package of subroutines for 6MV and 15MV photon beams. Experimental setup consists in the use of an extrapolation chamber (PTW model 23392), considered the most suitable instrument to measure absorbed dose in the build-up region, but its not commonly available in the hospitals because its use is not practical. The chamber was adapted for its use in clinical environments in a previous work, then for this work the measurement process is easier and results with high level of accuracy can be obtained.

In this way, EC (extrapolation chamber) measurements served as the gold standard in our study to validate the Monte Carlo simulations and also with results reported by previous studies. As a result, we found that simulation outcomes are in good agreement with experimental data.

Contents

List of Figures

List of Tables

Chapter 1

Introduction

External beam radiotherapy or teletherapy is the most common form of radiotherapy, the patient sits or lies on a couch and an external source of radiation is pointed at a particular part of the body. Then, radiation always interacts with the skin. Furthermore beam releases energy along its track and deliver an adequate dose to the tumor target is not possible without deliver a considerable amount of absorbed dose nearby critical normal structures, such as, basal layer on patients's surface. The importance in these type of treatments is to improve quality of life rather than cause distressing effects to patients; for this purpose quantification of skin dose is essential, as well as, the consideration of this region as a sensitive structure during treatment planning in order to reduce the skin toxicity to a tolerable level of damage without compromising tumor target coverage.

To quantify absorbed dose in the skin is difficult and not intuitive. The skin is within the buildup region, it is characterized by a lack of charged particle equilibrium that generates a rapid change of dose gradient, in addition, this region has a size of few centimeters, as a result, all dosimetric methods (dosimeters and simulations) have important limitations to give good results and available data has been obtained with a high degree of uncertainty. Mainly absorbed dose in the first few mm is due to electron contamination, these particles are originated by scattering photon interactions with components of the accelerator head, such as the secondary jaws, beam modifiers and the air around the accelerator; secondary contributions arise from interactions inside the patient's body.

The use of extrapolation chambers allows reliable measurements of dose in the build up region. In other hand, MC simulation is generally considered to be an accurate tool for dose estimation in radiotherapy since the beam's particles are tracked individually in the media. Therefore both methods may be employed in order to quantify the dose absorbed by the surface but is mandatory to do a comparison between results obtained by the two methods, taking into account their uncertainties. Finally, results should be contrasted against different measuring methods and experimental settings from the

literature although available results are limited. This lack of information shows the importance of this work and the results that will be obtained.

The main purpose of this work is to determine the percentage depth dose in the skin (depth at $z = 0.07\ mm$ according to ICRP regulations) for 6 MV and 15 MV photon beams from a VARIAN 2100CD medical linear accelerator. The work was focused on MC simulations carried out with the PENELOPE code and on measurements with an extrapolation chamber. Then, all simulated and measured data in terms of percentage depth dose (PDD) were compared.

Chapter 2

Background

Linacs (Linear particle accelerators) are usually mounted isocentrically and the operational systems are distributed over five major and distinct sections of the machine:

- Gantry (also called treatment head);
- Gantry stand or support;
- Modulator cabinet;
- Patient support assembly (i.e. treatment table);
- Control console.

The linac head contains several components that influence the production, shaping, localizing and monitoring of the clinical photon and electron beams. Electrons originating in the electron gun are accelerated in the accelerating waveguide to the desired kinetic energy and then brought, in the form of a pencil beam, through the beam transport system into the linac treatment head, where the clinical photon and electron beams are produced.

In order to generate a beam that can be used for patient treatment, electron beam must either be converted to photons or the narrow electron beam must be appropriately scattered with different features contained in the head of the accelerator (Schematic structure is in figure 2.1). For instance photon beam generation requires:

- **The X-ray target:** X-rays are generated by bremsstrahlung from a high energy electron beam striking a high atomic number metal target. Clinical photon beams are produced with a targetflattening-filter combination and each one has its own target-flattening filter combinations.

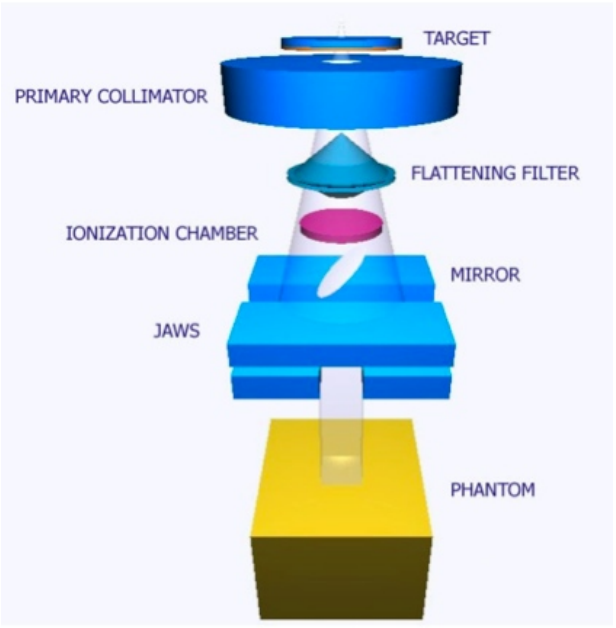

FIGURE 2.1: Diagram of a head accelerator.

- **The flattening filter:** This filter is used because the bremsstrahlung generated is mainly forward direct and it is necessary to compensate the lack of scatter at the edges of the field, so the filter enables designing a profile that increases toward the edges. The flattening filters are mounted on a rotating carousel or sliding drawer for ease of mechanical positioning into the beam, as required.

- **Collimation system:** Collimators are devices to constrain the radiation beam. They ensure that only the required part of the patient is irradiated. The primary collimator defines a maximum circular field that is further truncated with an adjustable rectangular collimator consisting of two upper and two lower independent jaws and producing rectangular and square fields with a maximum dimension of $40x40\ cm^2$ at the linac isocenter. Inevitably any type of those elements change the sharpness of the edges on the beam, as more primary beam particles interact with them more secondary particles are produced.

  Conventional collimators are not enough because they are only able to constrain the radiation to a rectangular shape. Nowadays multileaf collimators have been introduced allowing any beam shape to be produced subject to the width of the leaves, although at the same time, dosimetric characteristics as percentage depth dose, output factors and penumbra are modified by their use.

- **Dual transmission ionization chambers:** They are used for monitoring the photon and electron radiation beam output as well as the radial and transverse beam flatness.

- **Field defining light and a range finder:** It provides convenient visual methods for correctly positioning the patient for treatment using reference marks. The field light illuminates an area that coincides with the radiation treatment field on the patients skin, while the range finder is used to place the patient at the correct treatment distance by projecting a centimeter scale whose image on the patients skin indicates the vertical distance from the linac isocenter.

- **Beam modifiers:** Beam modifiers are referring to any kind of additional filter or bolus to modify the amount of dose that is delivered to the patients. Bolus is used for tissue compensation and increases effects of radiation scattered into the skin instead of compensating and wedge filters that are used to to achieve a homogenous dose distribution in the irradiated volume.

2.1 Physical aspects

Dose accumulated at the boundary between the air and the patient's skin is known as the surface dose. Although its value is less than the maximum absorbed dose achieved inside the patient, dose within the first few millimeters of the body is not negligible. Surface dose represents contributions to the dose from (Podgorsak and Kainz, 2005):

- Photons scattered from the collimators, flattening filter and air;
- Photons backscattered from the patient;
- High energy electrons produced by photon interactions in air and any shielding structures in the vicinity of the patient.

2.1.1 Buildup region

The buildup area (Figure 2.2) is a characteristic of a photon beam profile. Dose deposition sharply increases due to the deposited secondary electrons generated in the medium but they have finite longitudinal and lateral range (Metcalfe et al., 2007). The secondary electrons are Compton electrons at higher energies directly in the forward direction and release their energy further away from the point of interaction. Consequently, the number of electrons in each layer of the phantom rise until the point in which equilibrium is reached. Therefore the deposition of energy is almost uniform along their path; the electron equilibrium, in the case of megavoltage beam, is reached at the depth (in cm) where 1/4 of maximum energy expressed in MeV is laid down.

The amount of energy, which is deposited in the build up region, depends on several factors (See Figure 2.3):

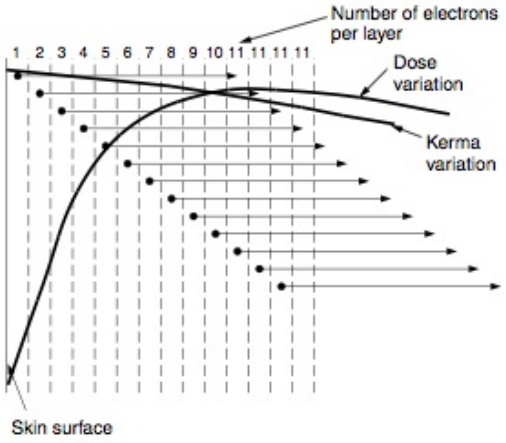

FIGURE 2.2: Idealised representation of buildup region (assuming no attenuation takes place)(Mayles et al., 2007).

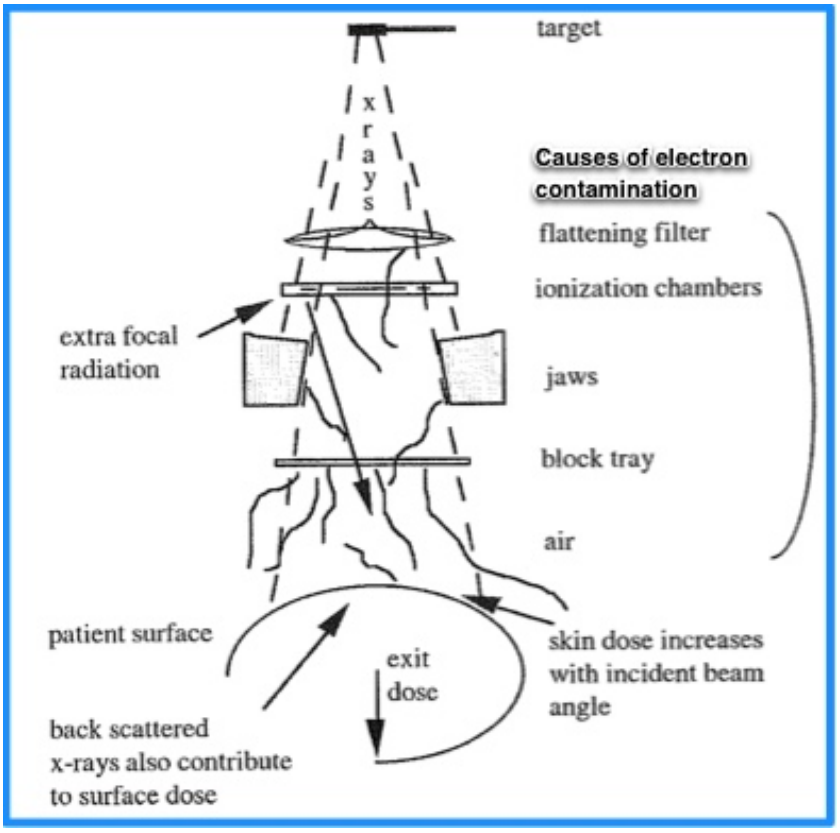

FIGURE 2.3: Contributions to patient skin dose from high-energy photon beams (Metcalfe et al., 2007).

- **Energy and field sizes:** Universally, the surface dose increases linearly with field size and simultaneously should be smaller at higher energies (See figure 2.4). However, it only happens for small field sizes, for field sizes above $10x10\ cm^2$ the surface dose may be greater at very high energies because main electron contamination is due to the flattening filter, as a result, the effect is increased by large fields and more energetic beams. In addition, as beam energy increases the depth of d_{max} (depth with maximum dose) increases.

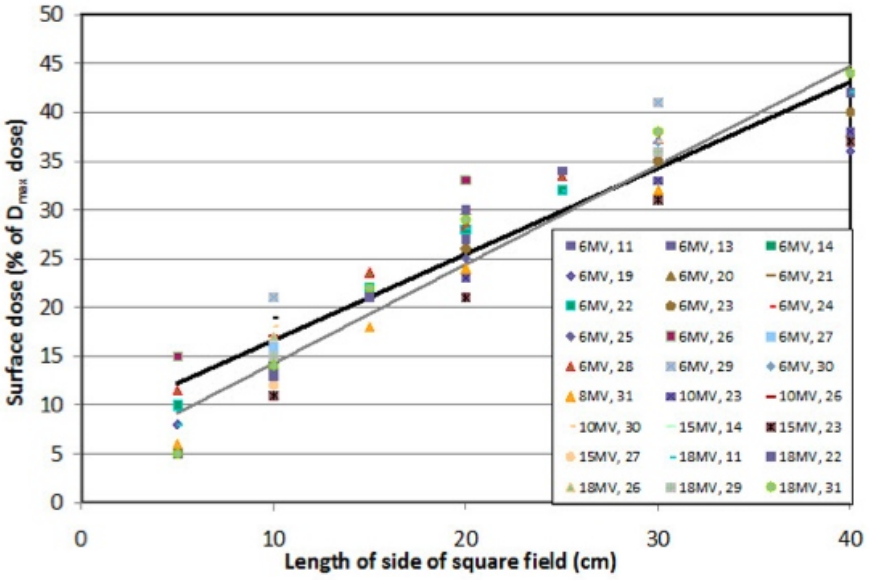

FIGURE 2.4: Percentage depth dose from open megavoltage fields (6MV-18MV) as a function of the size of the edge of the equivalent square field (Kry et al., 2012).

Dose to the entrance of the surface (on the central axis of the beam and approximately SSD of 100cm) is between $\sim$ 10% and $\sim$ 45% of the d_{max} dose (known historically as the given dose or entrance dose).

- **Beam-modifying devices:** There are two sources of contamination by secondary electrons and low energy photons. One is the treatment head linac and the other is the use of additional beam modifiers such as wedges, bolus or masks. The amount of these contaminant electrons and low-energy photons will affect the surface and the buildup region dose. For megavoltage beams, the surface dose increases with the presence of an acrylic or polycarbonate block tray particularly for large and open fields. This effect was dominant for large field sizes at lower SSD because them not always are fixed to the accelerator head, in those cases, the skin dose decreases significantly as the distance between block tray and the patient is reduced (Kry et al., 2012).

  Wedge filters, as their name implies, were originally metal wedges designed to produce the desired dose distributions. Beams modified by wedge filters are often described as wedged beams besides there are several variants of the wedge filter.

The filter (Figure 2.5) alters the beam quality by preferentially attenuation of the lower-energy photons (beam hardening) and, to a lesser extent, by Compton scattering, which results in energy degradation (beam softening). Those blocks are used because their material is transparent but electrons striking with them originate contamination. Collimating treatment field with blocks has only a small impact on surface dose besides to the impact of the block tray, it is because the production of secondary electrons from the acrylic block tray is more than eliminated by the tray, therefore, skin doses are increased.

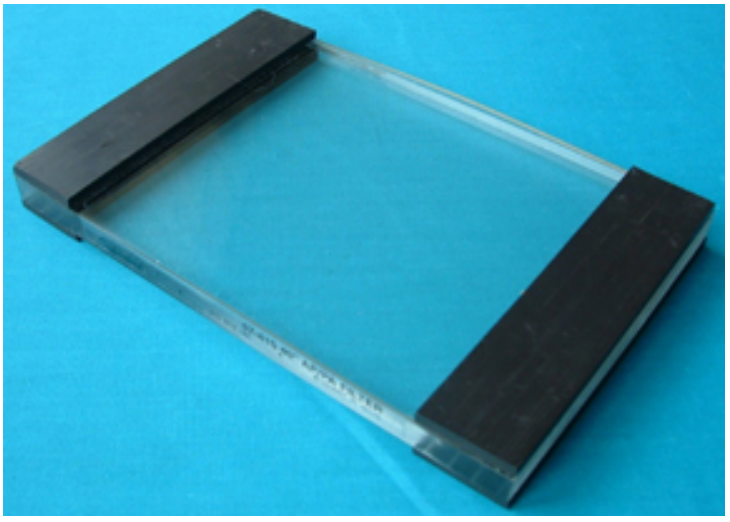

FIGURE 2.5: Wedge filter used in radiotherapy treatments.

Beam modifiers change the dose delivered to the surface. The increment in this value may cause early radiation effects such as erythema or late radiation-induced effects such as hypoxia and relangiecresia.

Additionally, immobilization devices or trays, such as thermoplastic masks (Figure 2.6) also increase the skin dose. Some measurements have shown that the mask had a bolus effect on the skin surface and it 'generates' an extra layer of skin. For instance, figure 2.7 shows the effect on dose distribution in the buildup region when a Lucite shadow tray is placed in the beam at various distances from the phantom surface, plot shows not only does the relative surface dose increases with decreasing tray to surface distance, but also the point of maximum dose buildup moves near to the surface.

- **SSD (Source-Surface distance) and setup:** SSD is a significant factor of the change of dose rate with depth. By increasing the distance between the tray and the surface, the electron fluence incident on the skin is reduced because of divergence, absorption and scattering of electrons in the air. On the other hand, the surface dose increases gradually while this distance decreases although the real effect is relatively small (Kry et al., 2012).

FIGURE 2.6: Thermoplastic mask designed for radiation oncology patient stabilization.

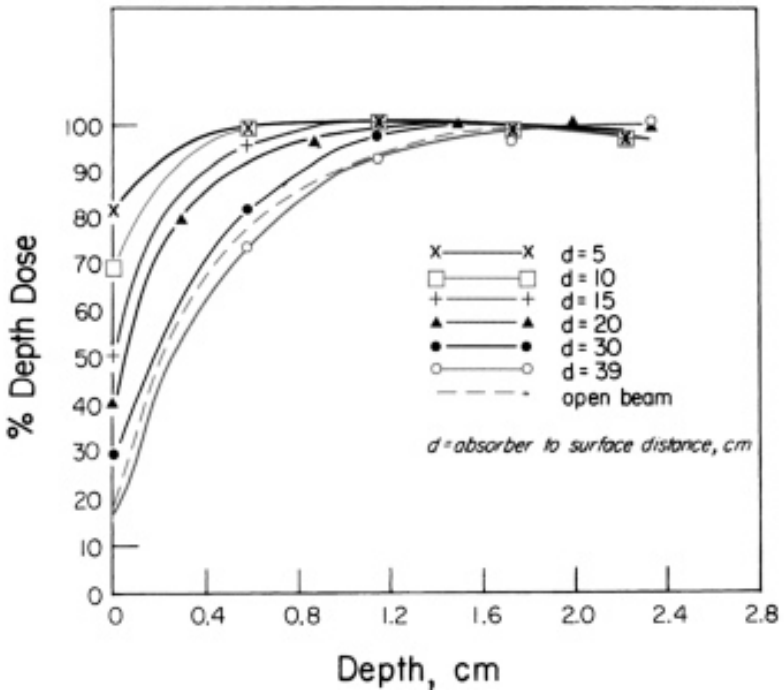

FIGURE 2.7: Effect of Lucite shadow tray on dose buildup for 10MV photons (Mayles et al., 2007).

- **Obliquity:** Beam obliquity as well as beam modifiers changes the dose delivered to the surface region due to changes in the scattering geometry, scattered photon and secondary electron production. It also changes the energy spectrum of the beam. Oblique beams incidences increase the surface dose, the behavior for small angles ($< 40°$) is almost imperceptible instead of large angles in which surface doses increase steeply. Some studies have shown that the percentage buildup dose has a much stronger dependence upon the angle of incidence than upon the effective wedge angle. For distances approaching the treatment head, the universal wedge mounted within the head treatment (used in some linear accelerators) generates secondary electrons that elevate the surface dose but this contribution decreases with distance.

- **Off-axis position:** Off-axis skin dose decreased as distance increased from central axis for fields with Perspex block trays. Surface dose is relatively uniform across field within the field size treatment field, however, it decreases slightly at the edge of the field. This decrease is typically less than a 10% relative decrease, but can approach a 30% relative decrease at the edge of the treatment field in the presence of beam modifiers (Kry et al., 2012).

- **Exit dose:** Approximately $50 - 70\%$ of applied dose was delivered to the skin on the exiting side of the beam for the greater part of patients . Exit dose delivered to skin consists of dose from forwardly scattered electrons. Dose to the exit surface is less than the predicted by the percentage depth dose PPD, that is when full scatter conditions are not achieved. The relative difference for most of megavoltage energies is about 15%.

- **Outside the treatment field:** Although great amount of data are not available for distances out field of the treatment, in many cases surface dose varies minimally with depth except near the surface where it reaches higher values (See figure 2.8). Actually, these values are 2 to 7 times greater that the dose a few centimeters below the surface. The ratio of surface dose to dose depth is larger for greater distances from the field edge and larger field sizes (Kry et al., 2012).

As the sum of factors listed, value of skin dose is not negligible but is not intuitive and difficult to measure.

2.2 Medical aspects

Skin dose is a value that may be of interest for clinical evaluation principally because the risk of acute and late effects in the patients (See Figure 2.9). Despite of the widespread

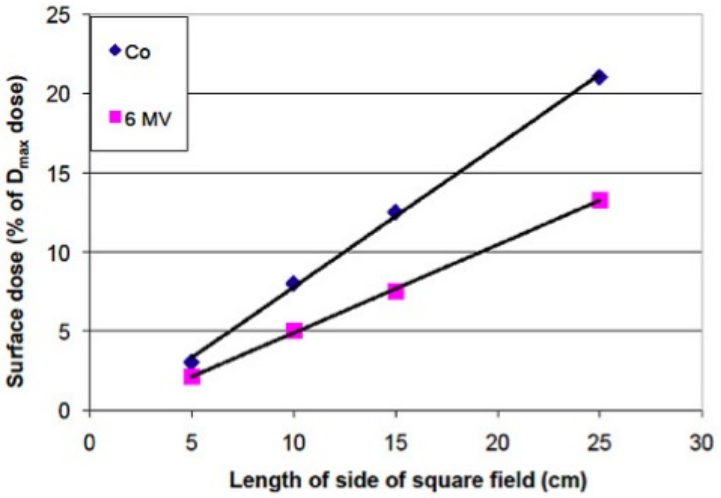

FIGURE 2.8: Percentage depth dose 2 *cm* from the field edge for a Co-60 beam and 6MV beam.

use of a linear accelerators and technologic advances in IMRT (Intense Modulated Radiation Therapy), the increase use of concomitant chemotherapy and high-dose treatments has remained skin reactions as a significant problem for patients.

In general, radiation reactions in this area can be divided into early or acute changes and delayed or chronic change. The epithelial reactions, should be characterized by the following 4 stages: erythema, dry desquamation, wet desquamation and necrosis; severity of the skin reactions depends on the dose given as well as the volume of the tissue irradiated (Lee et al., 2002), radiation skin reaction occurs at doses around 20-25 Gy or approximately 10 days into radical treatment. Previous studies (Buston et al., 2006) have concluded a marked increment in skin reactions: doses of 35 Gy increases erythema reactions, for desquamation an increase in incidence started at approximately at 37 Gy and finally telangectasia started at approximately 45 Gy and some patients presented permanent telangectasia after 51 Gy.

Skin dose can be plotted as the percentage of tumor dose as seen in figure 2.10. This figure highlights the field size dependence of skin dose with an increasing trend in absorbed dose with field size. Likewise, figure 2.11 shows the total absorbed dose delivered to the patient's basal cell and dermal layers for the entire treatment: doses ranges are from 2 Gy up to 45 Gy.

Although to estimate the true incidence of skin reactions is difficult and statistically available data predict a low occurrence of skin reactions, toxicity on it induced by radiation treatment affects most of the patients with breast, neck and head cancer. During last years interest in skin dose has been growing, the studies involve development of appropriate methods to prevent and to improve the quality of life of the patients rather than generate distressing side effects.

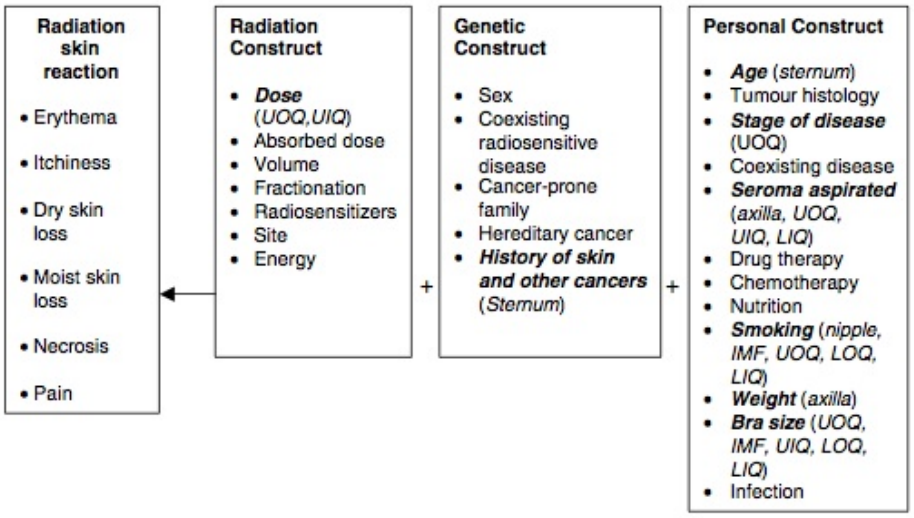

FIGURE 2.9: Conceptual framework of predictors of radiation skin reactions (UOQ, Upper outer quadrant; UIQ, upper inner quadrant; LIQ, lower inner quadrant; LOQ, lower outer quadrant; IMF, intrammary fold) (Wells and Macbride, 2003).

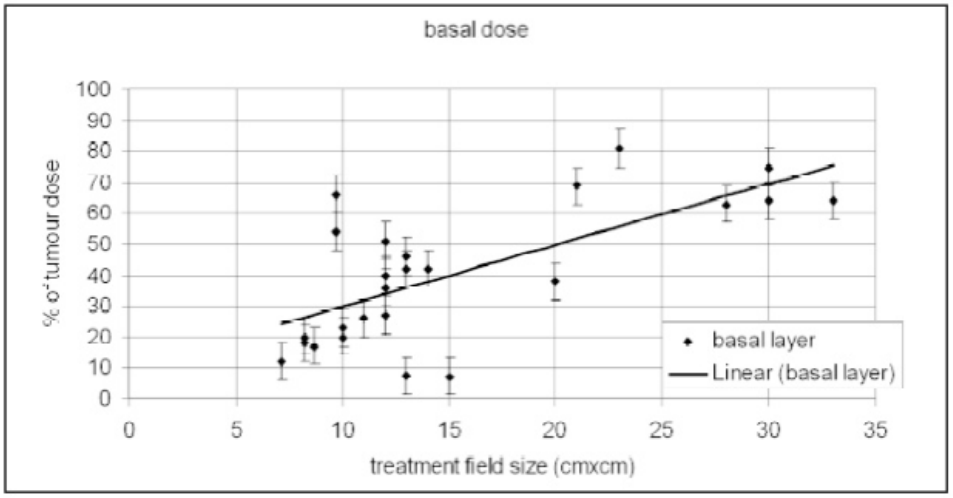

FIGURE 2.10: Dose delivered to the basal cell layer as a percentage of tumor dose (Buston et al., 2006).

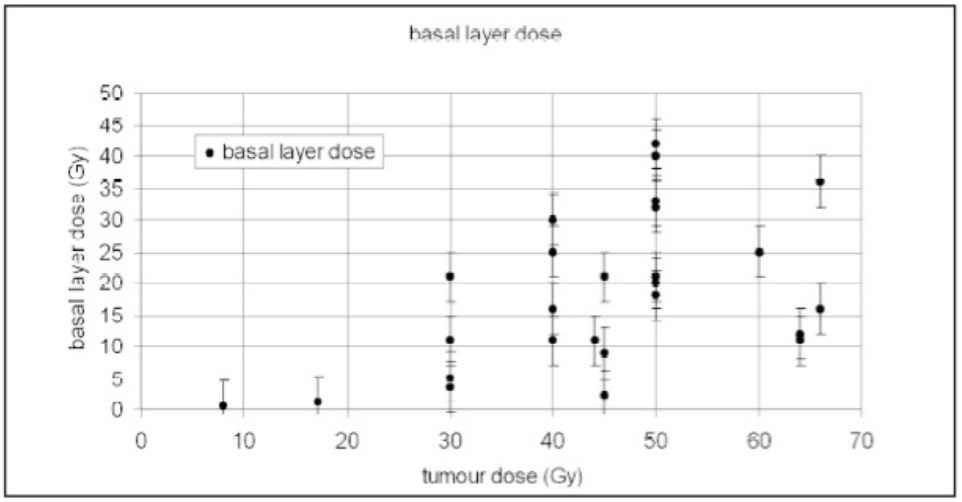

FIGURE 2.11: Total dose (Gy) delivered to the basal cell layer for 26 patients under going radiotherapy treatments (Buston et al., 2006).

2.3 Dosimetric techniques to quantify skin dose

2.3.1 Radiochromic films

Radiochromic films have been used to measure the absorbed dose (10^5-10^8 rads) due to the linear increase of its optic density as a function of deposited energy independently of dose rate.

These films are easy to manage and their design allows measurements over the phantom's surface rising accuracy and sensibility of the results. Use of radiochromic film in clinical environments is very common due to its small size, cost, and portability.

In order to determine skin dose, the process involves placing dosimeters on phantom's surface and they are irradiated with a similar amount of energy than the real treatment. Then, radiochromic films are analyzed making a comparison with the calibration curve and their values of optical density to determine absorbed dose. Additional materials around films are forbidden because they contribute to scattering interactions, it results in an over-response in the measurements.

2.3.2 Thermoluminescence Dosimeters TLD

TLD is the most common personal dosimetric method. Thermoluminescence materials have the property of storing energy and releasing in form of photons only where they are heated; the released energy is proportional to the stored energy. TLDs can measure only integrated dose since they must be allowed to absorb and store energy.

Those type of dosimeters show many advantages if they are used to quantify skin dose. Dose response is linear above of 10 Gy and measurement's time is very short (only few minutes), besides its material is tissue equivalent, as a result, data obtained are a good estimation of radiation dose in a given position and in a given radiation field on the patient. Extrapolation of the dose to an infinitesimal thin layer of LiF as well as interpolation between the different effective measurement depths is possible using TLD chips of three different thicknesses (See figure 2.12) (Kron et al., 1993).

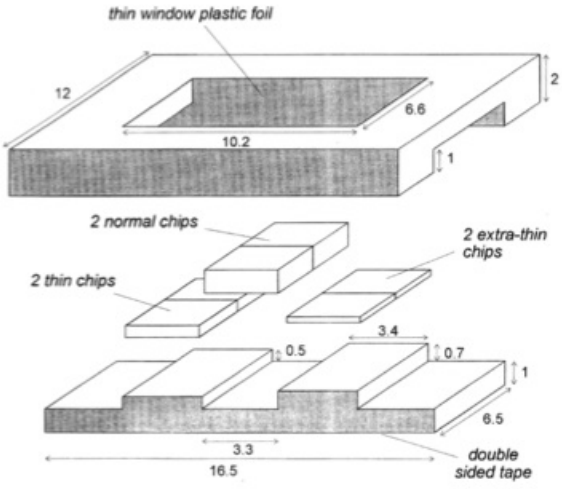

FIGURE 2.12: Schematic drawing of the TLD holder used in the study, all distances are in millimeters (Kron et al., 1993).

2.3.3 Ionization chambers

A ionization chamber (figure 2.13) consists of a gas-filled chamber with two electrodes (parallel planes or coaxial cylinders), a voltage potential is applied between the electrodes to create an electric field in the fill gas. When ionizing radiation interacts with the gas, pairs of charges are created and the resultant positive ions and dissociated electrons move to the electrodes of the opposite polarity under the influence of the electric field. This movement generates a current, which is measured by an electrometer.

These chambers have many advantages and are commonly available at hospitals but are not commonly adequate to use for the surface dose measurements in clinical situations. Their accuracy in the buildup region remains in doubt since there exists a cavity perturbation from the chamber volume that causes excess ionizations. To obtain a good result of absorbed doses in the buildup region, the readings need to be corrected taking into account perturbation conditions, furthermore correction factors have been proposed derived from aluminium-walled extrapolation chamber measurements. However, Nilsson and Montelius (Nilsson and Sorcini, 1989) showed that the application of

those correction factors to different chamber structures led to a significant error in the derived surface dose value.

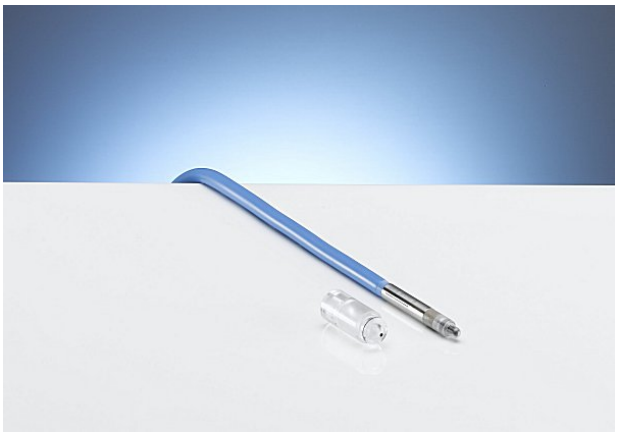

FIGURE 2.13: Waterproof ionization chambers for dose measurements in radiotherapy.

2.3.4 Extrapolation chambers

An extrapolation chamber (figure 2.14) is a type of parallel plane ionization chamber, capable to measure the differential specific charge by varying air mass in the cavity by the control of electrode separation. These chambers are designed for fields that have a uniform intensity across the area of the parallel plates, but vary sharply in the perpendicular direction and their response in the non-equilibrium region has good results. Therefore, the surface dose can be estimated by measuring the ionization per unit of volume as a function of electrode separation, and then extrapolating the data to a zero separation (Jayaraman, 2004).

Measurements of the charge collected per unit time per unit volume are obtained reducing gradually the distance between plates in a controlled way by a micrometer screw. A linear regression of electrode separation and collected charge values allows to relate the measurements with the absorbed dose in the region of interest. Unfortunately, the use of extrapolation chambers is limited since they are not available in most hospitals and institutes, additionally the measuring procedure is time-consuming.

2.3.5 Computational tools

Monte Carlo MC technique (See chart in figure 2.15) for the simulation of photons through media consists in use of the knowledge of the probability distributions governing the individual interactions of those photons in materials to simulate its random trajectories. One keeps track of physical quantities of interest for a large number of histories to provide the required information about the requested average quantities.

FIGURE 2.14: Extrapolation chamber PTW model 23392.

Simulation allows scoring datas as: average distance to interaction, number of primary and secondary particles of each type, energy deposited by them or more complex and useful quantities.

Nowadays several Monte Carlo codes have been developed for radiotherapy treatment planning, in general these type of simulations are considered a very accurate tool to estimate values of absorbed dose in different regions of interest. Studies related with surface dose have demonstrated the coherence between the results from MC simulations and the measurements obtained using an extrapolation chamber, then computational tools are considered an alternative and excellent method when surface or skin dose must be computed.

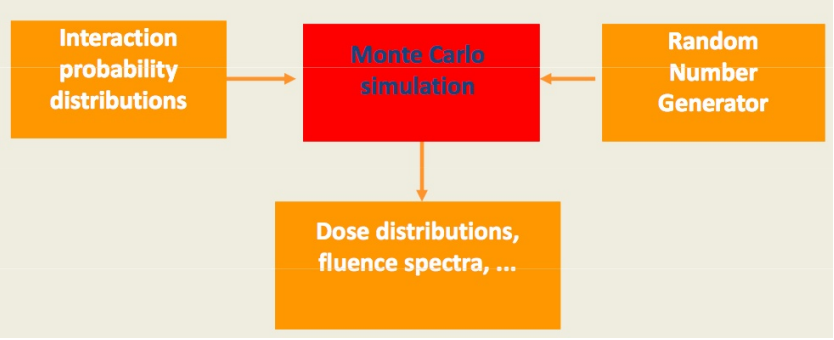

FIGURE 2.15: Important aspects of Monte Carlo simulation.

Chapter 3

Methods

3.1 Monte Carlo (MC) Simulations

MC methods are used in a great amount of applications where the user needs to provide a numerical solution to a problem, which can be described in terms of temporal evolution of objects interacting with other objects based on relations defined by a cross section values (For instance (Panettieri et al., 2009)). For this reason, the use of them in Medical Physics always has looked like a reasonable choice (Figure 3.1), because nature of radiotherapy treatments (accelerators, quantum particles, microscopic and macroscopic scale involve, etc) requires powerful simulation tools in order to obtain better dose predictions and dosimetry plans.

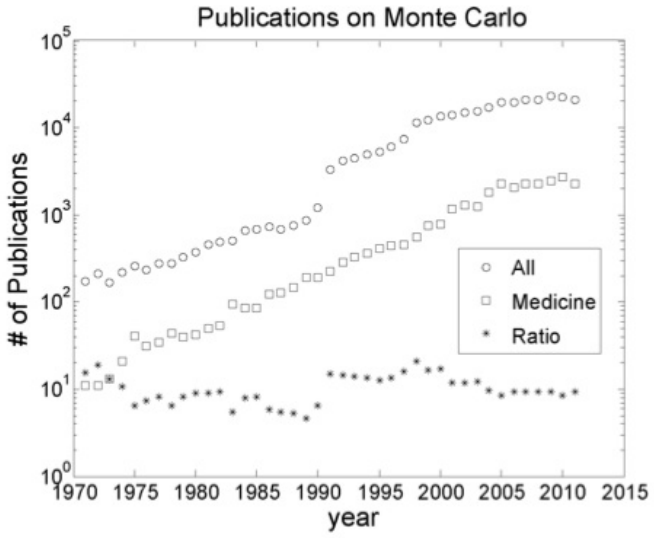

FIGURE 3.1: The number of papers published per year. Data acquire from Web of Knowledge ('All') and MedLine ('Medicine') (Bielajew and Carlo, 1991).

The MC method is generally considered to be an accurate tool for dose estimation in radiotherapy since beam's particles are tracked individually in the media according to a reliable interaction database (Apipunyasopon et al., 2013), now probably is an excellent option in the surface dose quantification. Results are suitable as in terms of accuracy as reproducibility and they are a source of reliable data.

In this work, all simulations were carried out with PENELOPE code system. It has been developed in the University of Barcelona and INTE (Institut de Tècniques Energètiques) of the UPC.

3.1.1 PENELOPE

Penelope is a package of subroutines, based upon Fortran, to simulate electron-photon transport within a wide range of materials between energies from a few hundred of eV to GeV. Photon transport is simulated by means of the standard, detailed simulation scheme. Electron and positron histories are generated combining a detailed simulation of hard events with a condensed simulation of soft interactions (Salvat et al., 2011). Respect to geometry the subroutine PENGEOM allows, through quadric surfaces, build homogenous bodies and modules, in which, the program generates cascades of photons interactions. After simulation running, available PENELOPE's results include: dose deposition, energy deposition, particle track structure and others more.

3.1.2 Main Program: PENEASY

A main program is required by PENELOPE, it must manage the geometry and evolution of radiation transport, keep track of relevant data and perform required averages at the end of the simulation. Some examples of main programs are supplied with the distribution package, but in this work penEasy have been used, it is a general-purpose main program for PENELOPE that has been successfully used in previous works (`inte.upc.edu/downloads`). It provides users with a set of source models, tallies and variance reduction techniques that are invoked from a structured code. PenEasy provides a modular code that facilitates the adaptation of routines to user needs without change the main program and users need only to input the required information through a configuration file. A scheme of the structure of *Peneasy.f* can be found in Appendix A.

General characteristics and implementation of each one of the modules used in this work are explained below:

3.1.2.1 Configuration section

The simulations were performed with $\approx 10^{10}$ histories and random seeds were left to its default value in the first trials, when the uncertainty of the simulation was higher, an external program calculated initialization values to produce independent results between simulations. SeedsMLCG program generates these pseudo-random values meanwhile other relevant parameters were preserved assuring independence of simulated events. This action is necessary because generated seeds are not really random, if a number is used as a seed more than once, machine would generate the same random numbers every time, that is the simulation would be the same. An example of the list of seeds generated with a program based on *RANECU* is presented in 3.1.
Aspect of this module inside penEasy.f subroutine is shown in Appendix A.

RANECU seed 1
670356969
420792192
1566905700
1765101456
1233408633

TABLE 3.1: Seeds generated from an arbitrary seed elected by the user.

3.1.2.2 Source section -PSF-

PSF (Phase-space file), as its name says, is a file, which contains the information of each beam's particle: position, direction, charge energy and weight; besides it reproduces the radiation field produced by a linear accelerator before entering into the patient. In this work, two sources had been used: 6 MV and 15 MV with a field size equal to $10x10\ cm^2$ and corresponding to a parameters fixed by a Varian Clinic 2100 C/D accelerator. Those PSFs were developed by previous projects and their validation process was successful completed. Aspect of this module inside penEasy.f subroutine is shown in Appendix A.

3.1.2.3 Geometry section -PENGEOM-

For current MC simulations, two phantoms were modeled. First, for the beam validation process, an homogenous $50x50x50\ cm^2$ water cube was build and simulated. Second one was a $30x30x20\ cm^2$ parallelepiped phantom of ^{TM}Plastic water to quantify skin dose.

To speed up the simulation and allow the simultaneous computation of the dose in different regions, ^{TM}Plastic water cube (figure 3.2) was modeled as four different parallelepipeds:

- Region 1: Between $z = 0\ mm$ and $z = 1\ mm$.
- Region 2: Between $z = 1\ mm$ and $z = 4\ cm$.
- Region 3: Between $z = 4\ cm$ and $z = 10\ cm$.
- Region 4: Between $z = 10\ cm$ and $z = 20\ cm$.

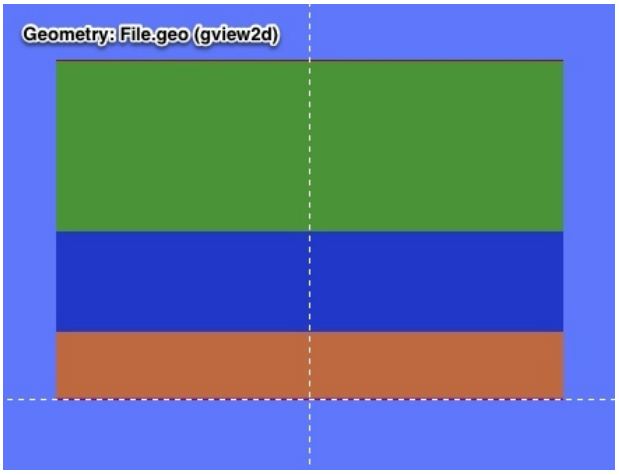

FIGURE 3.2: Cubes set up into phantom in order to compute skin dose.

Both geometry files with quadric surfaces are described with detail in Appendix A.

3.1.2.4 Penelope section

This module includes the identification of data files with the materials that are used in the different phantoms and elements of the simulation. Previously, the material must be generated by running of the program MATERIAL (included in Penelope package). A water predefined material was employed for beam validation, while in main simulations a material called ^{TM}Plastic water (composition is explained in table 3.1) was defined. In addition, air material is defined ensuring that the space between accelerator head and phantom is filled by it.

Element	Atomic Number (Z)	% Weight
C	6	0.5988
O	8	0.2354
H	1	0.0780
N	7	0.0176
Ca	20	0.0675
Cl	17	0.0022

TABLE 3.2: ^{TM}Plastic water composition

The transport algorithm for electrons and positrons in each material is controlled by the following parameters and they also affect the accuracy and speed of the simulation (See Table 3.3):

- EABS Local absorption energies for each one of the particles in the process (photons, electron and positrons). This feature can be used to reduce the simulation work in the regions of less interest.
- C1(M) Average angular deflection, produced by multiple elastic scattering along a path length equal to the mean free path between consecutive hard elastic events.
- C2(M) Maximum average fractional energy loss, between consecutive hard elastic events.
- WCC(M) Cutoff energy loss in eV, for hard inelastic collisions.
- DSMAX Parameter defines the maximum allowed step length for electrons/positrons; for photons, it has no effect.

To improve the speed of the simulation based on the same ^{TM}Plastic water material, different simulation parameters were set in the top region defined in the $30x30x20\ cm^2$ phantom, as defined in the previous section.

Material	EABS γ (eV)	EABS e^- (eV)	EABS e^+ (eV)	C1	C2	WCC (eV)	DSMAX
^{TM}plasticwater1	$10x10^3$	$100x10^3$	$100x10^3$	0.1	0.1	$100x10^3$	0.002
^{TM}plasticwater2	$10x10^3$	$100x10^3$	$100x10^3$	0.1	0.1	$100x10^3$	0.01
^{TM}plasticwater3	$10x10^4$	$500x10^3$	$500x10^3$	0.2	0.2	$100x10^3$	0.01
air	$10x10^3$	$100x10^3$	$100x10^3$	0.1	0.1	$100x10^3$	$10x10^3$

TABLE 3.3: Transport parameters used in the simulation

3.1.2.5 Tally sections

PenEasy provides different result tallies but in this work we have used the tally 'Spatial Dose Distribution'.

- **Spatial Dose Distribution:** Absorbed dose per simulated history can be calculated by this module in the main program, the dose is estimated using the collision estimator (scoring the energy deposited on the spot in each interaction) (Salvat et al., 2011). 3D distribution is obtained by the corresponding intervals and bins in each axis (x,y,z), spherical, cylindrical and as in our case parallelepiped bins can be used. The standard penEasy only allows the user to compute this tally with a defined bin spacing. To provide a simultaneous simulation at four regions of interest in the phantom, the code has been modified; tally was replicated four

times (See tally structure in Appendix A) each one of them is able to calculate, in an independent way, absorbed dose in the region where is defined.

This type of modification allows to have smaller regions over the phantom (in reference with beam's entrance) besides more bins are specified in order to obtain a better dose distribution in the first mm of tissue. Simulation has been performed with a variable size of bin in z axis but constant in x and y axes. Dimensions of x and y bins try to reproduce the window of the extrapolation chamber.

3.1.2.6 Variance-reduction techniques

In general, variance-reduction techniques are used to reduce statistical uncertainty of an interest quantity without increasing the computer simulation time. These methods are highly recommended in problems, such as skin dose determination, since only a particular region of the geometry defined is of interest in the simulation performance.

- **Interaction forcing**: Interaction forcing method artificially increases the interaction probability of process specified by the user, as a result, force interactions occur more frequently than for the real process. Interaction forcing can effectively reduce the statistical uncertainties of some simulation results (Salvat et al., 2011).

  To apply interaction forcing in this work, parameters associated with interaction probabilities must be changed, it will be applied to photon interactions (Table 3.3) and inside the material defined in the first millimeter of ^{TM}Plastic water phantom, reminding that for this work the skin region is at 0.07 mm depth. Additionally, forcing factor was the same for all types of interactions and its value was equal to two.

Rayleigh scattering
Compton interaction
Photoelectric interaction
Electron-positron pair production
Delta interaction
Auxiliary fictitious friction

TABLE 3.4: Available Photon interactions to apply interaction forcing.

- **Particle splitting:** This technique promotes flux of radiation towards the region of interest. As interaction forcing, splitting is useful in situations where only a partial description of the transport process is required. PENELOPE has three different modes of splitting. In agreement with the problem, simple mode was chosen; this mode creates copies inside splitting material that are identical to the original particle. The second variance reduction alternative that can be employed is Particle Splitting. This method creates a number of copies of the original particle

with a reduced statistical weight, in addition, technique is only applied a specified material, in our case *Material 1* placed in the ROI (Region of interest). Parameters in the module of main program appear in Table 3.4.

Parameters	Value
Splitting Material	^{TM}Plastic water 1.0 (first mm)
W_{in}	0.001
Splitting factor	5.0

TABLE 3.5: Parameters applying splitting section.

3.2 Extrapolation chamber

An extrapolation chamber is a parallel-plate ionization chamber, with a small sensitive volume, which can be varied. Measurements with extrapolation chambers are considered 'the gold standard' (most accurate test in medical terms) in surface dose estimations; although its use is unusual and impractical within clinical environments.

A perspex EC PTW Model 23392 is used (See general structure in figure 3.3). The specifications are given by: Chamber entrance window-0.0035 mm polyethylene terephtalate (PEDT, Hostaphan) mylar foil. The area of the entrance window is 0.66 mg/cm^2. The measuring volume can be varied between 0.353 to 7.422 cm^3 by moving the electrode using a piston operated by a micrometer screw. The distance between the electrodes is variable from 0.25 mm to 10.5 mm with the accuracy of parallelism being $+1$ μm, taken from (GmbH, 2012). Diameters of the entrance window and the rear electrode are 60.5 mm each; the rear electrode is made up of perspex and methyl methacrylate (PMMA), with a graphite coated surface.

There is a guard electrode with a width of 14.8 mm and an insulating ring with a thickness of 0.2 mm and a width of 0.2 mm. The design of the chamber is such that the leakage current is $< 10^{12}A$. For effective plate separation of 0.5 mm the saturation effect occurs at a voltage of $> 50V$ (99.5 %) for dose rates as high as 335 Gy/s. In addition the chamber was connected to an electrometer PTW UNIDOS with dual polarity, the leakage of the ionization measurement is as low as 1 pC.

Upon the basis of a previous project where a chamber with those characteristics was adapted and calibrated to perform experiments with a Varian Clinic 2100CD accelerator (in the Santa Creu i Sant Pau Hospital), in this work the skin dose and the PDD along the central axis of the ^{TM}Plastic water cube were measured.

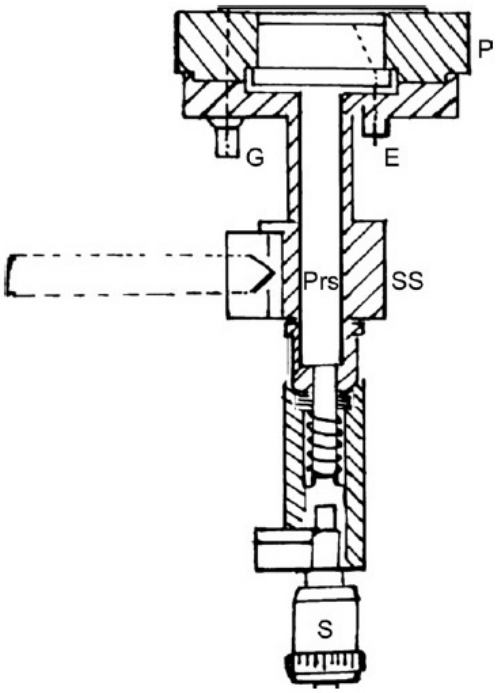

FIGURE 3.3: Schematic diagram of the extrapolation chamber (EC): G-ground, E-Bias voltage to collecting electrode, SS-Stainlees steel body, P-Perspex body, Pis-Piston, S-Micrometer screw.

3.2.1 Details of dose calculation

The Spencer-Attix air cavity relationship for the dose D_{med} in a phantom is (Zankowski and Podgorsak, 1997) :

$$D_{med} = \frac{Q}{m} W_{air} L_{air}^{med} \tag{3.1}$$

where Q is the charge collected under saturation conditions in the chamber sensitive air mass m, W_{air} is the mean energy required to produce an ion pair in air, and L_{air}^{med} is the ratio of restricted collisional mass stopping powers of the medium and air for the electron spectrum at the position of the cavity.

In the case of the volume in the cavity of the extrapolation chamber, it is very small then the ratio Q/M as a function of m is constant, allowing that this term will be replaced by one easier to.measure: derivate dQ/dm. As a result, the modified Spencer-Attix relationship for the dose to the medium can be written as:

$$D_{med} = \frac{dQ}{dm} W_{air} L_{air}^{med} \tag{3.2}$$

or for parallel-plate ionization chambers (an extrapolation chambers also):

$$D_{med} = (\frac{1}{\rho A})\frac{dQ}{dz} W_{air} L_{air}^{med} \tag{3.3}$$

where ρ is the density of air in the cavity, A is the effective area of the measuring electrode and z is the separation between the polarizing and measuring electrodes.

Although Equation 3.3 looks like a simple equation since majority of the terms are constant, computation of associated values carries many correction factors and the process raises level of uncertainty over absorbed dose value (See in detail (Hernández, 2012)).

3.2.2 Technical aspects

Percentage depth doses along the beam central axis for 6 MV and 15 MV photon beams should be acquired experimentally with the extrapolation chamber in a reproducible way. It has to be in horizontal position beneath head accelerator; for both energies square field size, geometry and SSD (source-surface distance) are the same. It means, distance between head's LINAC and the surface of the phantom must be 100 cm. All parameters are in agreement with the conditions of MC simulations. Figure 3.4 is the view of the EC and the LINAC arrangement.

FIGURE 3.4: Experimental arrangement at the hospital: Extrapolation chamber and LINAC.

3.2.3 Geometry of the measurements

Extrapolation chamber with its support are laid in horizontal position under head accelerator. To evaluate absorbed dose in deep, measurements are performed at various

depths from 1 mm until 15 mm or 30 mm depending on beam energy by keeping the ^{TM}Plastic water slabs on the surface of the entrance window of the EC, ensuring always a SSD (Source-Surface distance) of 100 cm (See figure 3.5 and figure 3.6).

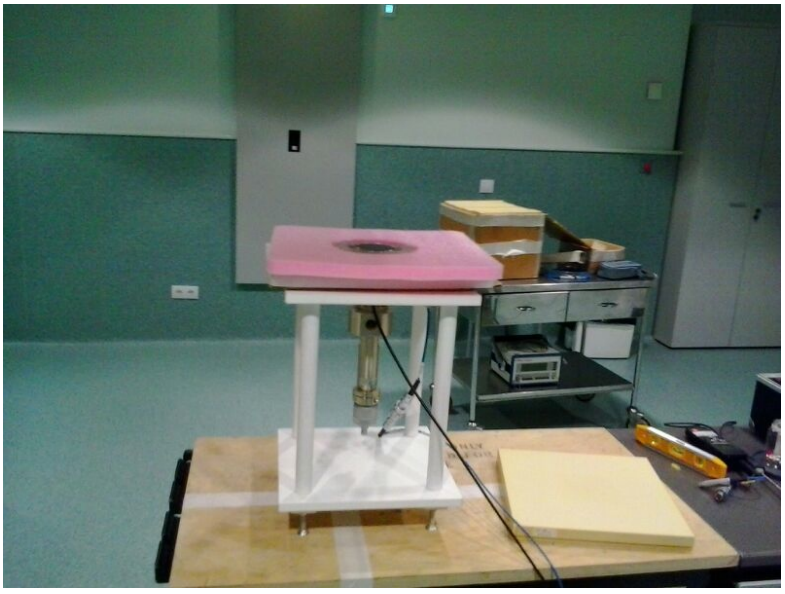

FIGURE 3.5: Geometry of measurements in deep of the absorbed dose with extrapolation chamber view 1.

FIGURE 3.6: Geometry of measurements in deep of the absorbed dose with extrapolation chamber view 2.

A reference field of $10x10$ cm^2 is used at the isocenter for both photon beams, in this manner MC parameters and empirical method are developed under similar conditions. Measurements were taken only at three different distances for chamber plate separation: 2.0 mm, 1.5 mm, and 0.5 mm according to the optimization in measurement protocol proposed by (Hernández, 2012). The ionization charge is collected for 10 MU (monitor

units) exposures. For each depth, ionization charge was measured at the positive and negative bias voltage finally the average was taken for each setting.

3.2.4 Optimization measurement's protocol

As has been pointed out in a previous work, the results with the highest accuracy were obtained when the measurements are taken for ten different plate separation, thus measurements obtained by extrapolation chambers in general are time consuming (up to 2 hours to measure only for the surface dose) and unpractical in clinical environments. The idea proposing a protocol is to ensure uncertainties below 2% with a lower quantity of registered measurements.
This work used a set of three measurements for each separation distance of the plates in both cases: negative and positive polarization of the chamber. This can be done taking into account that the important value to be measured is the slope of the linear regression between collected charge and chamber electrodes distance separation. Previous project, demonstrated values of reached uncertainty did not exceed 2% with this method in almost any probable combination of distances capable to be chosen by the user.

Chapter 4

Results

4.1 Monte Carlo simulations

4.1.1 Beam Validation

First step in the process was the validation of PDD (Percentage Depth Dose) curves. Results obtained with MC simulations by comparison against experimental PDD values for a $50x50x50$ cm^3 cubic water phantom in both cases of energies are shown in Figures 4.1 and 4.2.

Since this work is focused on the build-up region, materials and geometry for MC simulations were changed. Subsequently, validation process was performed with a $30x30x20$ cm^3 complex ^{TM}Plastic water phantom.

4.1.2 PDD within first mm -without modifications-

MC simulation was performed without substantial changes. Tally *Spatial Dose Distribution* was replicated four times, then attention could be focused within first mm in depth along the central axis within the phantom (See Figures 4.3 and 4.4). Main program code is the same for a 6 MV and 15 MV photon beams with their PSFs (Phase Space Files) respectively.

To give the surface or skin dose value means to analyze percentage doses at specific depths inside the phantom. Certainly, relevant depth of a measurement depends on which biological effect is of interest, although the layer recommend for practical dose assessments is situated at 0.07 mm depth according to ICRP (Nilsson and Sorcini, 1989). In this work for all cases, PDDs values at surface, at 0.07 mm and at 0.5 mm are observed in order to make comparisons with published results in previous studies.

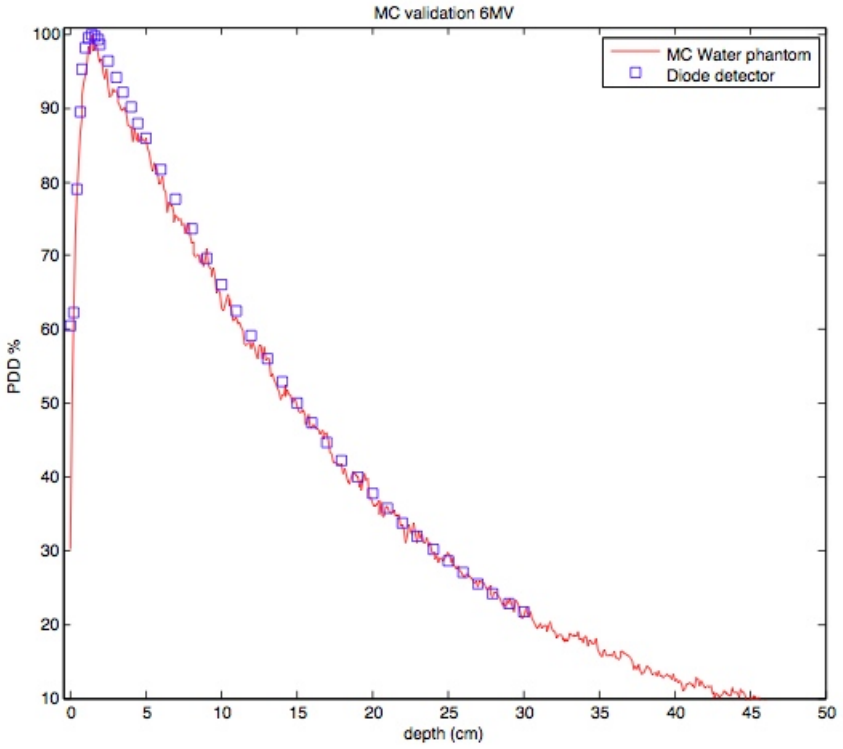

FIGURE 4.1: MC validation for 6 MV beam, water phantom, 10x10 cm^2 field size at SSD=100cm.

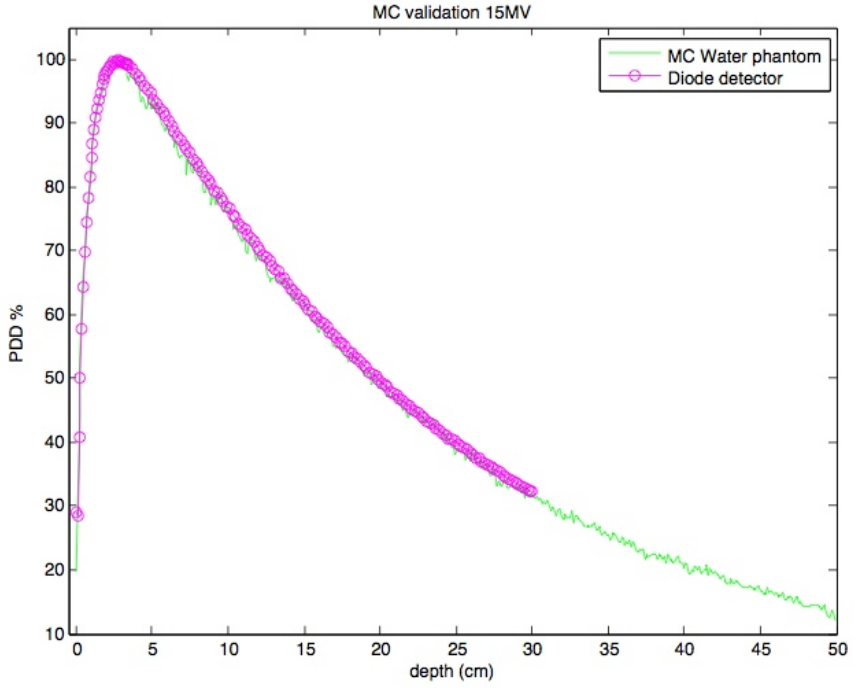

FIGURE 4.2: MC validation for 15 MV beam, water phantom, 10x10 cm^2 field size at SSD=100cm.

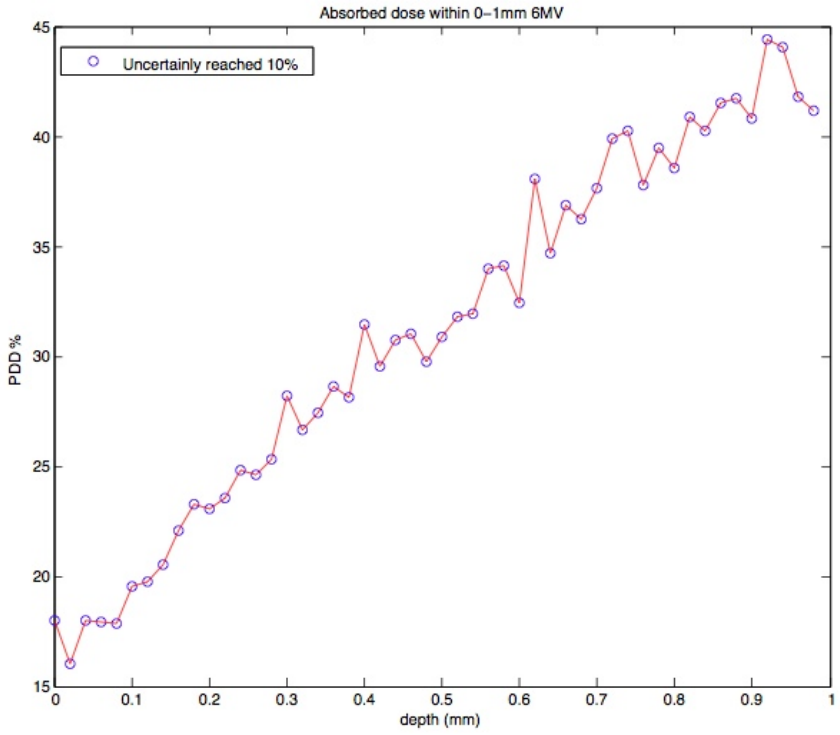

FIGURE 4.3: Absorbed dose for 6 MV. Uncertainty=10%.

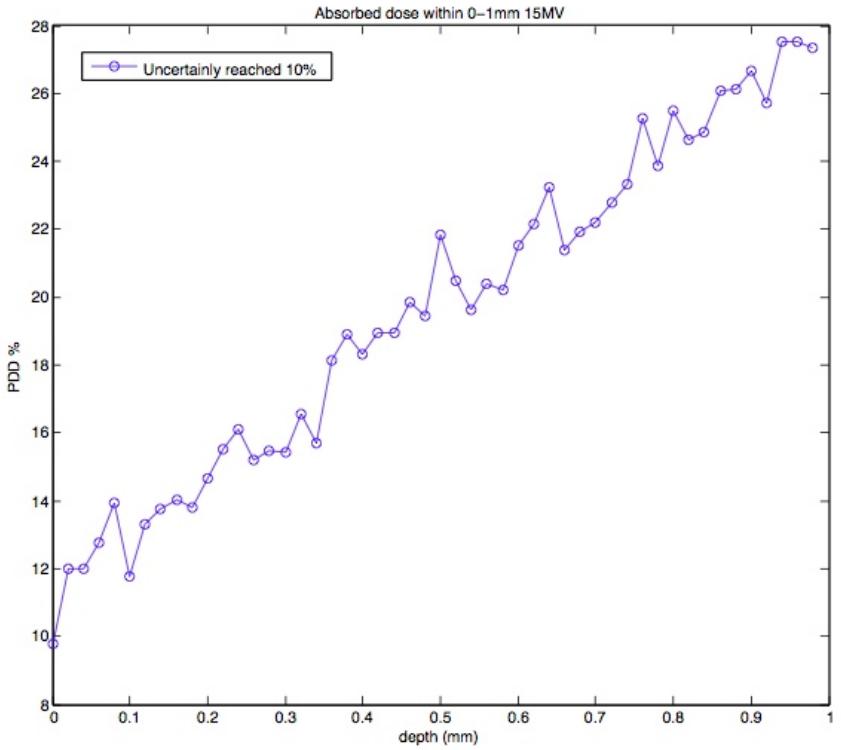

FIGURE 4.4: Absorbed dose for 15 MV. Uncertainty=10%.

First simulation reaches an average uncertainty of 10% and spends 4 days running in the Argos cluster. Results are shown in Table 4.1.

Depth (mm)	Energy (MV)	PDD (%)
0	6	18.02
	15	9.80
0.07	6	18.52
	15	12.78
0.5	6	33.51
	15	21.85

TABLE 4.1: Calculated doses in the plastic water phantom (Average reached uncertainty=10%).

4.1.3 PDD within first mm -(VR Variance Reduction Techniques-)

Uncertainty in the simulations above was too high and plots of the results have many fluctuations if they were compared with total absorbed dose curve. To obtain better results than the trials performed until now, variance reduction techniques may be employed. These techniques ensure a decay in the statistical uncertainty without increasing the computer simulation time. PENELOPE has available three types of VR methods but in this work only two have been tested.

- **Interaction forcing:**

  First available method in the main program PenEasy is interaction forcing, it consists to increase interaction probability of the different process, in which one type of particles are involved. Applying interaction forcing upon all photon interactions within material one (first mm of the phantom are filled with it), 5% of average uncertainty is reached. The depth dose curve comparison for the simulation without forcing and the simulation with forcing is shown for 6 MV in Figure 4.5 and for 15 MV in Figure 4.6. Table 4.2 summarizes calculated PDD values, their uncertainties and the difference in reference with previous MC simulations at specific depths of interest.

Depth (mm)	E (MV)	Not VR (%)	u_{PDDnot}(%)	Forcing(%)	u_{PDDfor} (%)	Diff
0	6	18.02	18	17.13	8	-0.89
	15	9.80	14	10.42	6	+0.62
0.07	6	18.52	13	17.73	6	-0.79
	15	12.78	14	11.52	6	-1.26
0.5	6	33.51	10	32.92	5	-0.59
	15	21.85	10	20.51	5	-1.34

TABLE 4.2: Comparison percentage dose values obtained with/without interaction forcing methods.

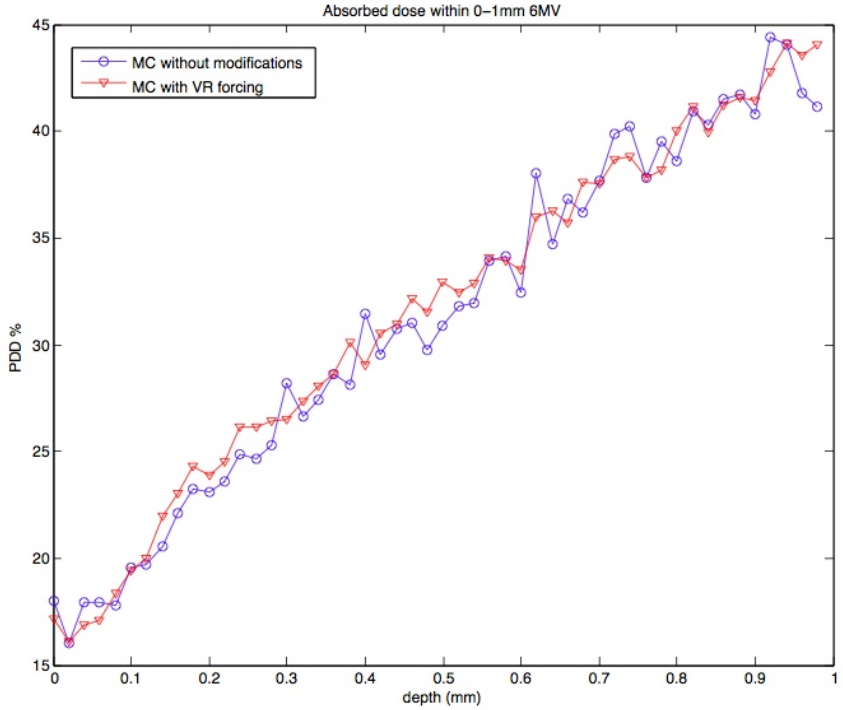

FIGURE 4.5: Comparison between MC simulations with/without interaction forcing method 6MV.

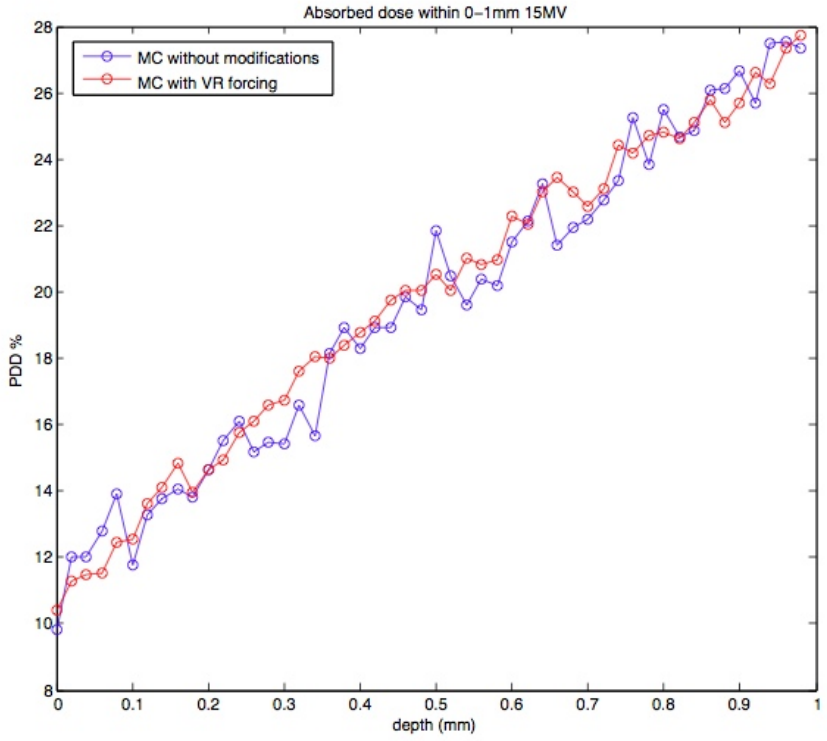

FIGURE 4.6: Comparison between MC simulations with/without interaction forcing method 15MV.

As the results show, implementation of forcing allows to achieve a better statistics in the same time of simulation (about three days running in ARGOS cluster of the INTE). However, the idea is obtaining results from MC simulations with the lowest possible uncertainty, they can be compared more precisely with the measurements using extrapolation chamber.

- **Particle Splitting:** *Particle splitting* and *interaction forcing* were applied, the number of copies or splitting factor was set as five. Depth dose curve comparison for the MC simulation using interaction forcing and MC simulation using both: forcing and splitting is shown in Figure 4.7, for 6 MV and in Figure 4.8 for 15 MV.

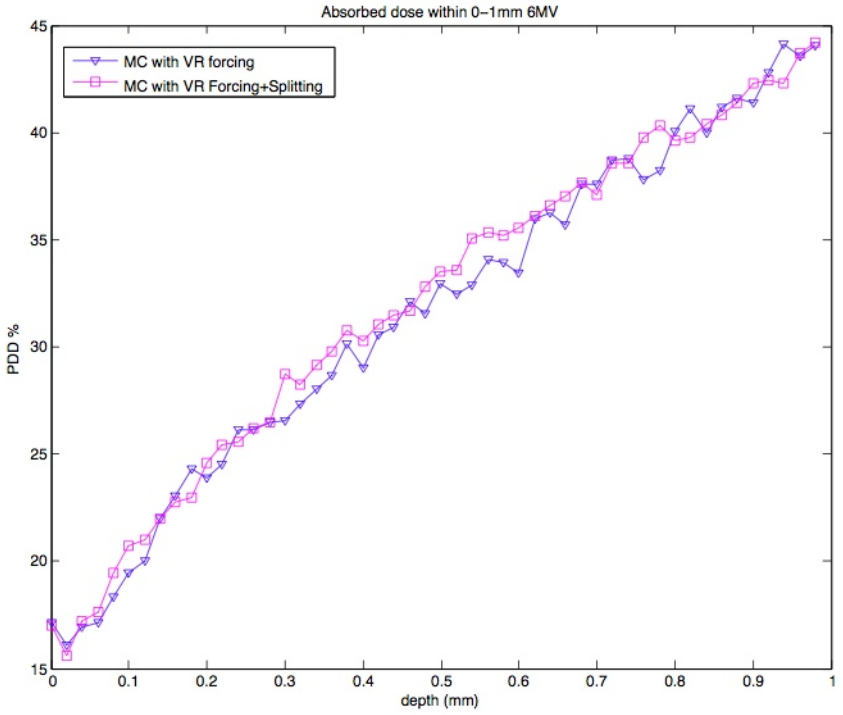

FIGURE 4.7: Comparison between MC simulations: interaction forcing and forcing plus splitting 6MV.

The first simulation combining forcing and splitting methods, the uncertainty reached values of 4% for 6 MV beam and 2% for 15 MV beam. Plot shows trend-lines alike in the region between 0 - 0.3 mm. From there, data corresponding to both VR methods are a little bit higher. Table 4.3 summarizes simulation results.

If attention is paid at depth of 0.07 mm, difference would be the highest in the set of analyzed distances along beam central axis. In advance of trying another techniques in order to improve statistics of the simulation in the case of 6 MV's beam (with worse reached uncertainty); forcing and splitting was applied once more setting the relative uncertainty of tally *Spatial Dose Distribution* to a lower value.

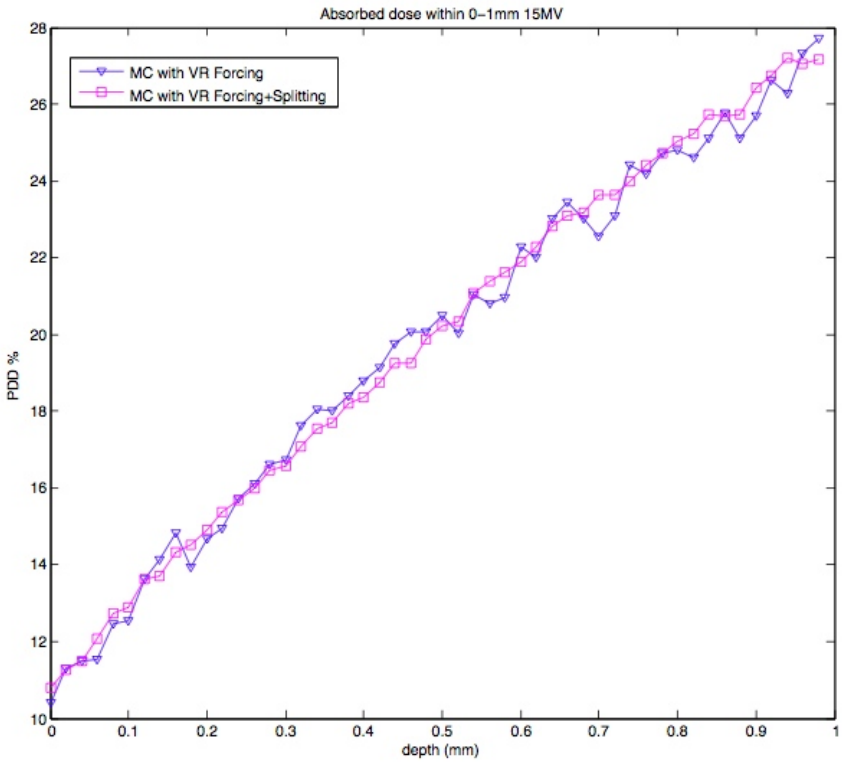

FIGURE 4.8: Comparison between MC simulations: interaction forcing and forcing plus splitting 15MV.

Depth (mm)	E (MV)	Forcing (%)	u_{PDDfor}(%)	For+Split(%)	u_{PDD2}(%)	Diff
0	6	17.13	8	16.98	10	-0.15
	15	10.42	6	10.80	2	+0.38
0.07	6	17.73	6	18.52	6	+0.79
	15	11.52	6	12.08	2	+0.56
0.5	6	32.92	5	33.51	5	+0.59
	15	20.51	5	20.21	2	-0.3

TABLE 4.3: Comparison percentage dose values obtained with two combinations of variance reduction techniques.

Figure 4.9 shows the results for splitting and forcing methods with two different uncertainties reached. Respect to numerical values, these are very similar despite time machine that can be double for 3% of requested uncertainty. At this point, other method is needed to improve accuracy of simulations.

4.1.4 PDD within first mm -Parallel Monte Carlo simulations-

Another effective method to improve errors of the results is performing independent Monte Carlo simulations with the control of the seeds. It ensures independence of parallel trials, those seeds are generated by an external program and they allow Monte

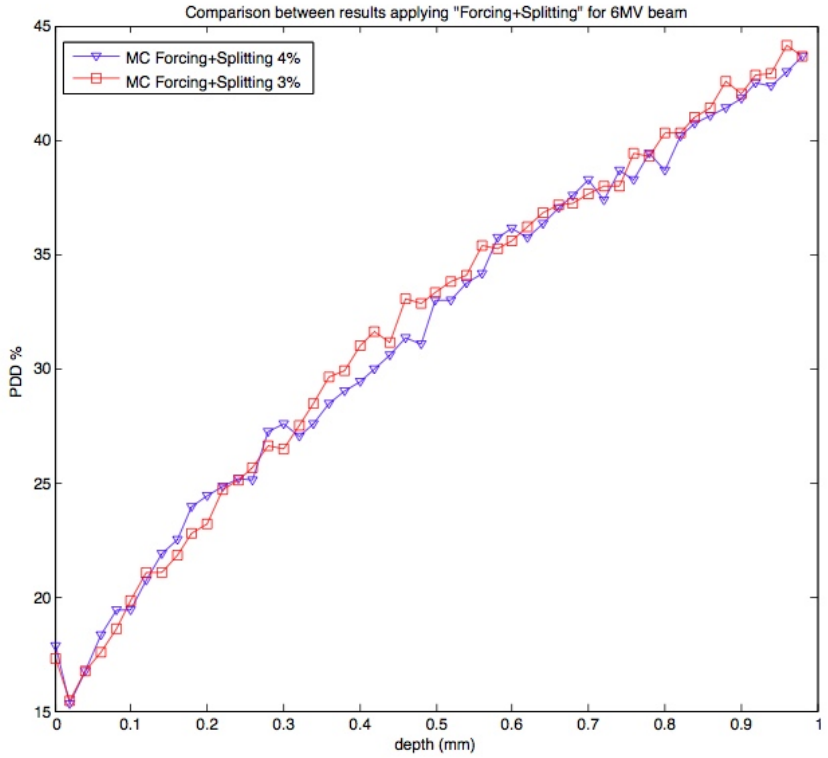

FIGURE 4.9: Comparison between results applying forcing and splitting methods for 6 MV.

Carlo simulations strictly reproducible. Results are shown in Figure 4.10 for 6 MV and in Figure 4.12 for 15 MV.

Absorbed dose at different depths (results per single run and mean value with its sample standard deviation) are summarized in Table 4.4. As one can conclude, final result has a lower uncertainty, which is given by Eq. 4.1.

$$s_{\overline{PDD}} = \frac{\sigma_{\overline{PDD}}}{\sqrt{N}}) \tag{4.1}$$

Depth (mm)	**Energy (MV)**	$PDD(\%)$ **each seed**					$\overline{PDD}(\%)$	$s_{\overline{PDD}}$
0	6	17.84	17.79	17.51	17.80	17.74	17.74	0.13
	15	10.94	10.52	11.03	10.67	10.70	10.77	0.21
0.07	6	18.30	18.12	18.44	18.53	18.32	18.35	0.15
	15	12.09	12.40	12.30	12.21	12.28	12.26	0.12
0.5	6	32.96	33.24	32.87	32.88	33.22	32.83	0.37
	15	20.26	19.88	19.85	20.30	19.84	20.07	0.30

TABLE 4.4: Summary the results of parallel simulations and definite absorbed dose value took into account in order to compare with extrapolation chamber measurements.

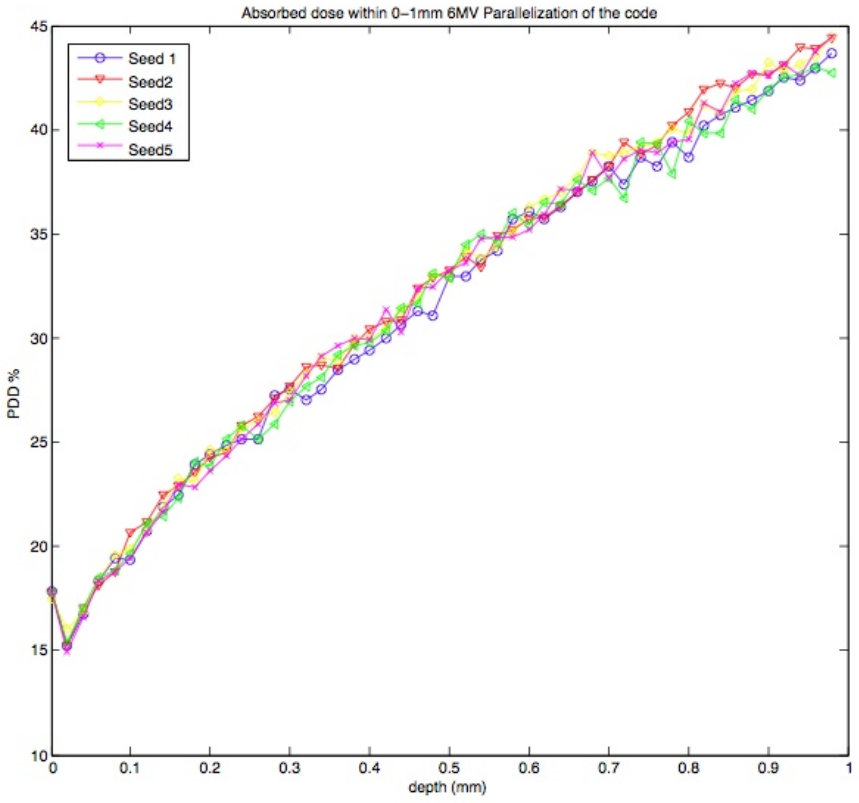

FIGURE 4.10: Percentage depth dose curves for different trials in parallel simulations for 6MV.

4.2 Extrapolation chamber measurements

Tables 4.5 and 4.6 show the summary of results in terms of collected ionization charge in pC for three different plate separations: 0.5 mm, 1.5 mm and 2 mm; obtained using micrometer screw adjustments. Data were taken under similar ambient conditions (Temperature: 297.5 K and Pressure: 100.95 kPa) and polarization voltage varies with plate separation. Moreover the readings from each measured position at the positive and negative bias voltage were averaged; the mean value and uncertainty of each measurement also can be found in this table. This uncertainty should be determined from standard deviation of the charge measured by:

$$u_{\overline{Q}} = \frac{\sqrt{s^2_{\overline{Q+}} + s^2_{\overline{Q-}}}}{2} \tag{4.2}$$

where $s_{\overline{Q+}}$ and $s_{\overline{Q-}}$ are the sample standard deviations of $Q+$ and $Q-$ mean values, respectively.

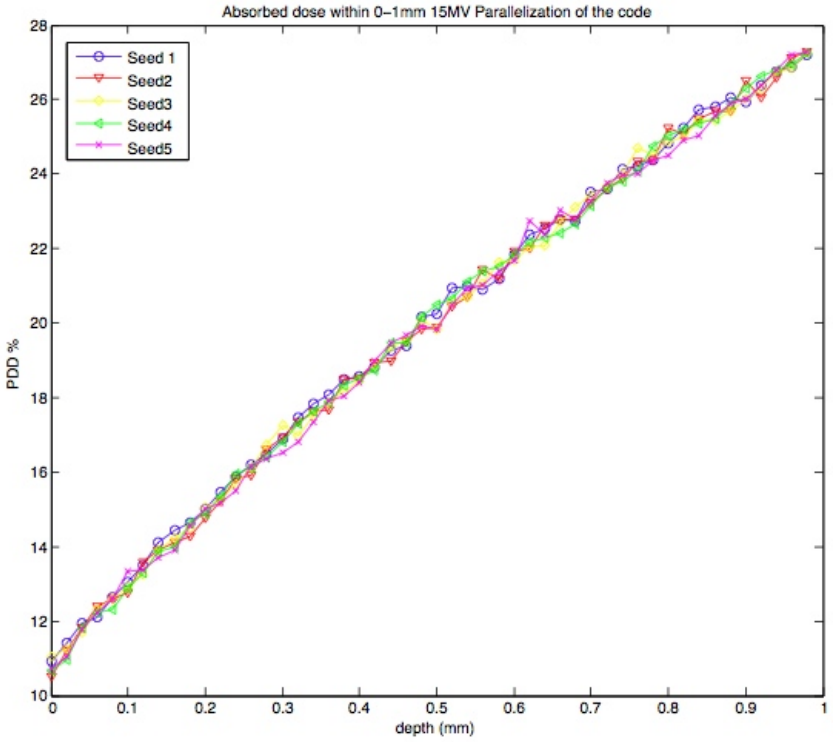

FIGURE 4.11: Percentage depth dose curves for different trials in parallel simulations for 15MV.

E(MV)	**Depth(mm)**	**d(mm)**	**V**	**Q(+) (pC)**	**Q(-) (pC)**	$\overline{Q}$ **(pC)**	u (pC)
6	0.0	2.0	20	1118	711	911.33	4
				1103	711.0		
				1114	711.0		
		1.5	15	903.0	482.5	691.38	2
				902.0	481.0		
				899.3	481.0		
		0.5	5	545.5	69.00	306.25	2
				542.0	70.00		
				541.0	70.0		
6	1.0	2.0	20	2854	2339	2639.0	41
				2841	2481		
				2838	2481		
		1.5	15	2321	1949	2129.0	4
				2313	1942		
				2306	1943		
		0.5	5	1236	892.00	306.25	2
				1240	886.50		
				1237	885.00		

E(MV)	**Depth(mm)**	**d(mm)**	**V**	**Q(+) (pC)**	**Q(-) (pC)**	$\overline{Q}$ **(pC)**	u (pC)
				3727	3451		
		2.0	20	3711	3453	3585.3	4
				3717	3453		
				3035	2743		
6	2.0	1.5	15	3018	2744	2881.8	6
				3035	2743		
				1576	1320		
		0.5	5	1578	1375	1445.3	3
				1570	1313		
				4664	4530		
		2.0	20	4754	4480	4612.3	26
				4732	4514		
				3840	3613		
6	4.0	1.5	15	3822	3615	3704.5	29
				3823	3514		
				1995	1763		
		0.5	5	1986	1755	1872.0	5
				1979	1755		
				5133	4860		
		2.0	20	5094	4829	4976.0	14
				5093	4850		
				4116	3895		
6	5.0	1.5	15	4096	3869	3988.5	11
				4089	3866		
				2135	1890		
		0.5	5	2139	1882	2010.0	3
				2131	1883		
				5500	5233		
		2.0	20	5482	5230	5345.3	21
				5457	5170		
				4464	4193		
6	7.0	1.5	15	4433	4202	4320.3	8
				4443	4197		
				2317	2153		
		0.5	5	2308	2137	2209.3	28
				2217	2124		
				5761	5446		
		2.0	20	5773	5501	5595.2	52
				5594	5496		
				4683	4448		
6	10.0	1.5	15			4541.5	27

E(MV)	**Depth(mm)**	**d(mm)**	**V**	**Q(+) (pC)**	**Q(-) (pC)**	$\overline{Q}$ **(pC)**	u (pC)
				4671	4433		
				4584	4430		
		0.5	5	2420	2200	2312.8	13
				2412	2190		
				2415	2240		
6	15.0	2.0	20	5880	5624	5740.7	9
				5855	5616		
				5846	5623		
		1.5	15	4740	4534	4624.2	10
				4730	4520		
				4711	4510		
		0.5	5	2478	2237	2349.0	6
				2470	2222		
				2459	2228		

Table 4.5: Summary the results of extrapolation chamber measurements for 6MV beam.

E(MV)	**Depth(mm)**	**d(mm)**	**V**	**Q(+) (pC)**	**Q(-) (pC)**	$\overline{Q}$ **(pC)**	u (pC)
15	0.0	2.0	20	982.5	544.0	761.16	2
				975.0	546.0		
				825.0	416.5		
		1.5	15	825.0	416.5	618.25	2
				819.5	416.5		
				818.0	414.0		
		0.5	5	517.0	145.0	330.58	1
				517.0	145.0		
				514.0	145.0		
15	1.0	2.0	20	2000	1521	1755.8	4
				1988	1517		
				1988	1521		
		1.5	15	1631	1174	1399.2	2
				1625	1169		
				1626	1170		
		0.5	5	930	470.5	700.33	1
				929.0	469.0		
				933.0	470.5		
		2.0	20	2648	2261	2445.66	10

15 2.0

E(MV)	**Depth(mm)**	**d(mm)**	**V**	**Q(+) (pC)**	**Q(-) (pC)**	$\overline{Q}$ **(pC)**	u (pC)
				2642	2227		
				2637	2259		
		1.5	15	2148	1786	1957.3	13
				2142	1780		
				2102	1786		
		0.5	5	1170	517.5	838.66	5
				1168	512.0		
				1164	500.5		
15	4,0	2.0	20	3598	3266	3416.2	18
				3589	3201		
				3582	3261		
		1.5	15	2944	2602	2763.2	7
				2926	2595		
				2925	2587		
		0.5	5	1562	1223	1381.7	14
				1561	1215		
				1557	1172		
15	5.0	2.0	20	3972	3620	3797.5	8
				3962	3640		
				3979	3612		
		1.5	15	3236	2862	3045.3	4
				3227	2853		
				3228	2866		
		0.5	5	1726	1359	1539	2
				1718	1359		
				1718	1359		
15	7.0	2.0	20	4504	4167	4332.5	3
				4504	4156		
				4503	4161		
		1.5	15	3673	3345	3503.6	7
				3679	3333		
				3675	3316		
		0.5	5	1966	1639	1796.3	5
				1963	1628		
				1963	1629		
15	10.0	2.0	20	5096	4740	4612.3	76
				5094	4471		
				5068	4726		
		1.5	15	4126	3810	3934.3	48
				4121	3637		

E(MV)	**Depth(mm)**	**d(mm)**	**V**	**Q(+) (pC)**	**Q(-) (pC)**	$\overline{Q}$ **(pC)**	u (pC)
				4120	3792		
		0.5	5	2157	1840	2007.0	9
				2183	1830		
				2182	1850		
		2.0	20	5553	5264	5408.3	4
				5560	5265		
				5544	5264		
		1.5	15	4520	4162	4356.3	14
15	15.0			4527	4209		
				4510	4210		
		0.5	5	2375	2072	2222.7	3
				2381	2066		
				2376	2066		
		2.0	20	5785	5173	5511.8	24
				5811	5234		
				5802	5266		
		1.5	15	4794	4524	4645.8	12
15	30.0			4781	4520		
				4767	4489		
		0.5	5	2496	2233	2359.5	5
				2496	2226		
				2492	2214		

Table 4.6: Summary the results of extrapolation chamber measurements for 15MV beam.

4.2.1 Temperature and Pressure correction factor

The charge measured by the chamber depends on the air temperature, pressure and humidity. Further, chamber signal should be corrected to normal conditions ($T_n = 20°C$ and $P_n = 101.325kPa$) then the factor may be applied for the particular ambient conditions is:

$$\gamma(P_k, Tk) = \frac{101.325kPa(273.15 + T_k)}{P_k(273.15 + 20°C)} \tag{4.3}$$

Correction factor allows convert the measured signal to the reference (normal conditions) used for the extrapolation chamber calibration at the standard laboratory. Value obtained in this case of temperature and pressure is $\gamma(P_k, Tk) = 1.02$.

Since now, measurements from extrapolation chamber will be shown here include the multiplication by this correction factor.

4.2.2 Values of $\frac{dQ}{dz}$ in deeper

From equation 3.3, derivate of chamber capaciting charge respect to chamber depth is related with absorbed dose. In this work, PDD profile will be determined directly from EC measurements saving the use of correction factors, for this purpose a linear regression was used to fit each set of data corresponding to different depths or thickness of the slabs over the chamber (Details obtaining and using linear regressions and extrapolation slopes are in Appendix B). Resultant slopes, it means absorbed dose equivalent values, are shown in Table 4.7.

Energy (MV)	**Depth (mm)**	$\frac{dQ}{dz}$ **(pC/mm)**
6	0.0	408.77
	1.0	1089.9
	2.0	1454.8
	4.0	1864.1
	5.0	2017.4
	7.0	2121.5
	10	2252.5
	15	2308.4
15	0.0	313.48
	1.0	720.12
	2.0	1000.0
	4.0	1382.9
	5.0	1531.6
	7.0	1732.1
	10	1981.0
	15	2162.6
	30	2165.0

TABLE 4.7: $\frac{dQ}{dz}$ obtained from EC measurements for each photon beam energy at each depth.

Depths in which absorbed dose is a maximum were reached at: $z = 15\ mm$ and $z = 30\ mm$ for each case of photon beam energy respectively.

4.2.3 Comparison with previous measurements in surface under similar experimental conditions

Preliminary results of PDD at the surface were determined by (Hernández, 2012). A comparison between both measurements is convenient in order to determine accuracy and similarity of results, reminding the main purpose of both projects is toward to the

same objective: Quantification of skin dose in a radiotherapy treatment. A summary of the values and the differences in terms of percentage found are presented in Table 4.8.

Energy (MV)	**PDD %**		Difference
	Hernandez, 2012	Valencia, 2013	
6	16.2	17.7	+1.5
15	14.3	13.5	-0.8

TABLE 4.8: Summary the results in order to compare EC measurements under same experimental conditions.

For both energies, good agreement between both experiment trials is found. Although photon beam difference is higher in 6 MV, their values are compatible within uncertainties of each one of the measurements.

4.2.4 PDD curves obtained from experimental data

Percentage depth doses along the beam central axis for 6 MV and 15 MV photons were acquired experimentally with extrapolation chamber (Figure 4.12). The readings in terms of collected charge for different plate distances were fitted using a linear regression as was explained before. Consequently, PDD profiles can be build normalizing value of $charge/mm$ at each depth respect to values obtained for the points, in which the dose is a maximum.

4.3 Comparison PDDs from MC simulations and empirical measurements

Now with experimental measurements obtained and MC simulations performed, is time to make a comparison between the results focusing on the near surface region. Both resultant percentage depth dose curves are plotted in order to correlate available data (Figures 4.13 and 4.14).

At first sight, in the case of 6 MV photon beam almost all possible depths from both methods are in good agreement. For 15 MV gradual changes are observed, probably the most significant disagreement corresponds to value at $z = 15\ mm$, percentage difference between the extrapolation chamber reading and MC simulation is around $6 - 7\%$. Although, further along beam path (near to d_{max}) values are alike.

Results in the first 2 - 3 mm should be highlighted because curves are in excellent agreement for both energies, PDD values nearby to surface seem match closer.

Table 4.9 summarizes calculated and measured doses at depth of 0.07 mm and 1.0 mm in the ^{TM}Plastic water phantom for 6 MV and 15 MV photons, respectively. The

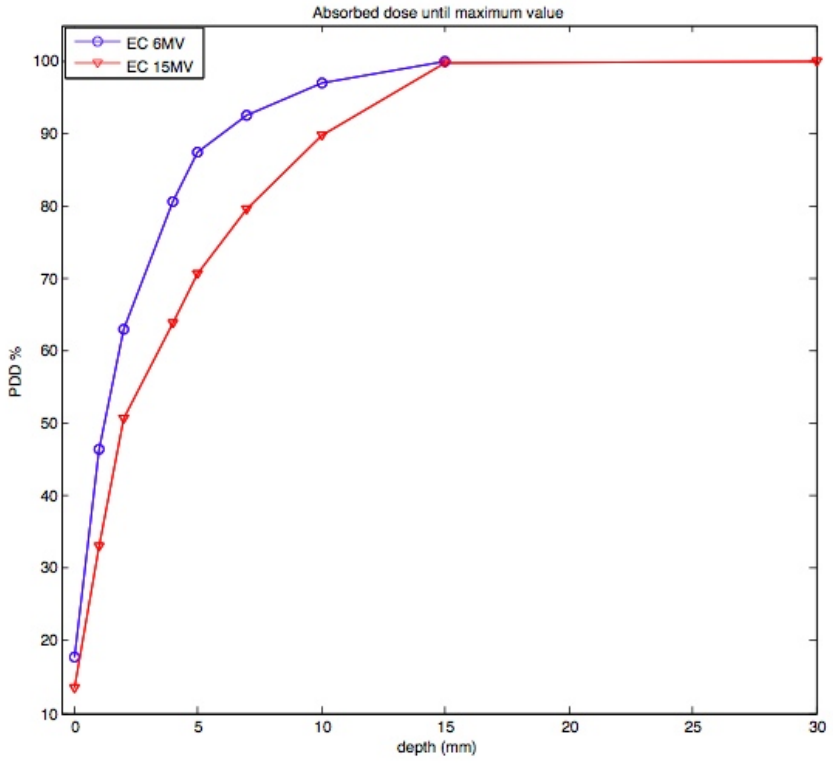

FIGURE 4.12: Percentage depth dose curves obtained using Extrapolation chamber.

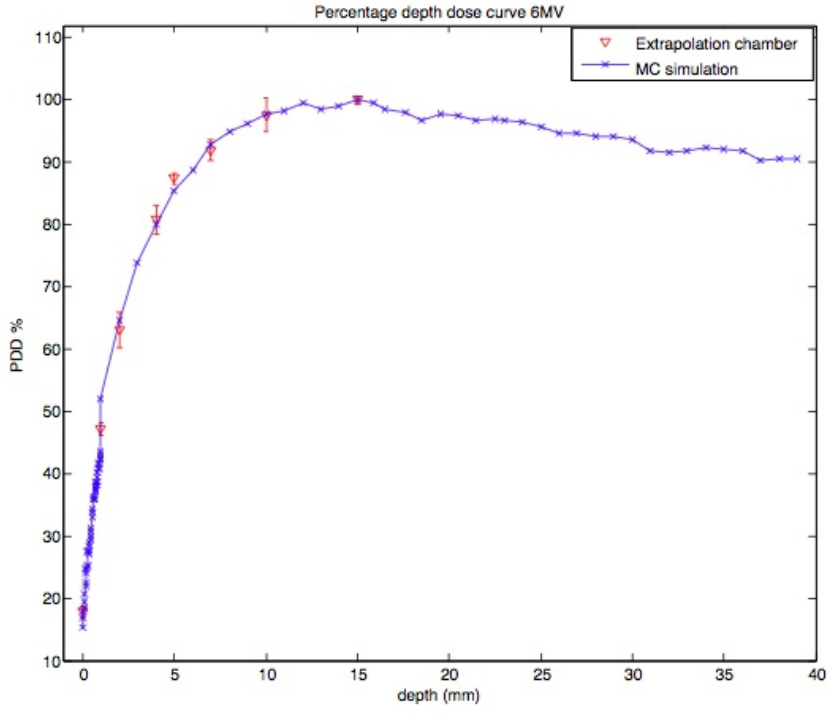

FIGURE 4.13: Percentage depth dose in the buildup region measured by extrapolation chamber compared with MC simulation results for 6MV.

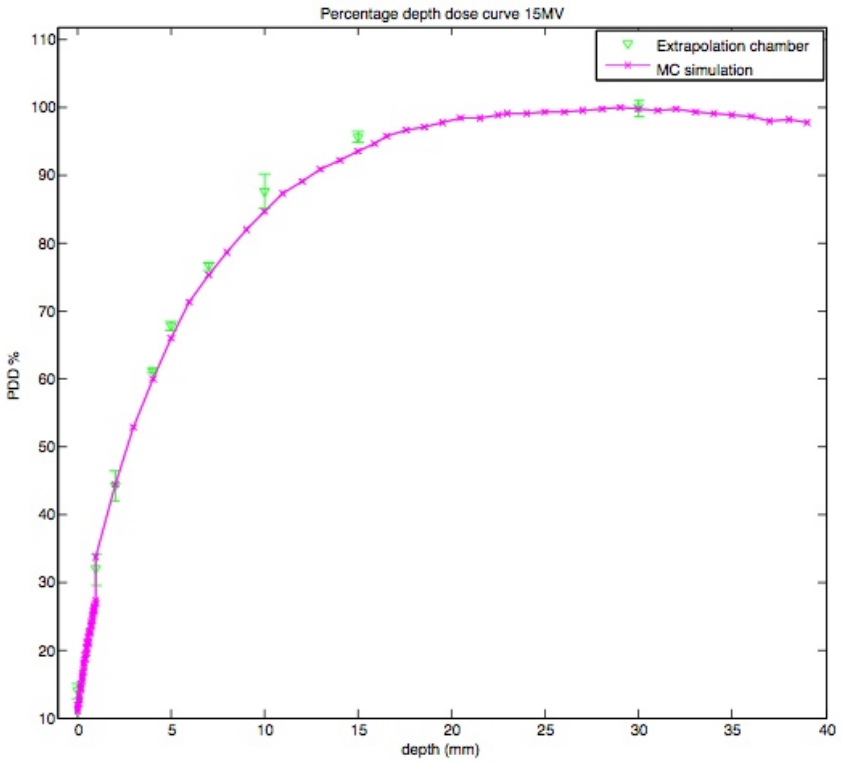

FIGURE 4.14: Percentage depth dose in the buildup region measured by extrapolation chamber compared with MC simulation results for 15 MV.

difference column is calculated to be the percent difference between the EC reading and MC simulation results for each pair of data.

Energy (MV)	Depth (mm)	EC (%)	MC (%)	Difference (%)
6	0.07	17.7	18.4	+0.6
	1.0	46.5	52.0	+6.0
15	0.07	13.5	12.3	-1.2
	1.0	33.0	33.6	+0.6

TABLE 4.9: Summary of calculated and measured PDDs for 6MV and 15MV photon beams.

For 6 MV the maximum deviation is within $5-6\%$ at 1 mm of depth inside the phantom, decreasing to below 1% nearby to the position of d_{max}. In the other hand, results for 15 MV photons are a little bit different.

Absorbed dose in the surface region decreases with energy of the beam as was expected. It happens because depth dose maximum z_{max} is proportional to the beam energy and this value depends on the highest amount of energy and range reached by secondary particles: electrons and positrons. This particular behavior is known in medical physics as skin-sparing effect (maximum energy is delivered in the sub epidermal region) and it is directly proportional to energy of the photons.

4.4 Comparison between results and reports in previous works

We can compare PDD at the skin to those available from previous studies performed under the same characteristics. Commonly is easier to find the PDD values for 6 MV beam because measurements for 15 MV have not been performed in the most of the cases. Table 4.10 summarizes these data and the difference column is calculated to be the percent difference corresponding report and our result, the results are comparable to all values found in the literature within uncertainties reached.

E(MV)	Type of work	Accelerator	PDD (%)	Diff (%)
6	Extrapolation chamber (Valencia,2013)	Varian 2100CD	17.7	0
	TLD Extrapolation(Kron et al., 1993)	Varian 2100C	16.3	-1.4
	Black TLDs (Thomas and Palmer, 1989)	Varian 2100C	19.3	+1.6
	Markus chamber(Rawlinson et al., 1992)	Varian 2100C	14.7	-3.0
	Extrapolation chamber(Rikner and Grusell, 1987)	Varian 2100C	14.9	-2.8
	Extrapolation chamber(Apipunyasopon et al., 2013)	Varian 23EX	16.0	-1.7
	Extrapolation chamber (Ishmael Parsai et al., 2008)	Varian 1800	16.4	-1.3
15	Extrapolation chamber (Valencia,2013)	Varian 2100CD	13.5	0
	Markus chamber(Yadav et al., 2010)	Elekta Precise	11.7	-1.8
	Ultra thin TLDs(Lin et al., 2001)	Siemens Primus	10.6	-2.9

TABLE 4.10: Percent depth dose (PDD %) of skin of different measured methods and accelerators from the literature.

Chapter 5

Conclusions

Quantification of absorbed dose in regions near to the patient skin is difficult and few data is available considering the importance of this quantity in the planning of radiotherapy treatments and the wide range of accelerators and beam energies used. Moreover buildup region, as is known the region within the first mm along beam releases its energy inside a phantom, has a particular characteristic of non electronic equilibrium. The use of an extrapolation chamber is always suggested to give an accurate value of dose in this region but results are also limited, experimental setup is troublesome to perform and this chamber is not typically available in most of the institutes and clinical environments.

The idea in this project was to evaluate MC simulations derived calculations beneath of first mm along path of the photon beam to demonstrate a possible coherence between the results and the measurements obtained using an extrapolation chamber. PenEasy, main program to manage the different simulations through PENELOPE, needed modifications in order to obtain an accurate value of PDD within the first mm of a parallelepiped ^{TM}Plastic Water phantom. First at all, four replications of tally Spatial Dose Distribution were made. Secondly, variance reduction techniques, in this case, interaction forcing and splitting factor, were used to enhance efficiency, time of running and accuracy of the simulation. Finally, looking for better statistics, Parallel MC simulations were performed ensuring independence of each single running; in this form the average reached uncertainty was around $\sim 4\%$.

On the other hand, measurements with an extrapolation chamber were carried out aver a Varian2100CD LINAC. The importance of the experimental method in this work unlike previous reports was to determine the percentage depth dose along beam's central axis until d_{max} (depth at which dose is a maximum) because additional equations or correction factors were not required.

Final objective consisted to compare calculated and measured PDD at surface, specially at depth of $z = 0.07$ mm (recommended layer for practical skin dose assessments according to ICRP) in the ^{TM}Plastic Water phantom for 6 MV and 15 MV photons respectively.

Results are: 17.7% measured, 18.4% calculated for 6MV and 13.5% measured , 12.3% calculated for 15MV. The maximum percent difference is $\sim$ 1% corresponding to the highest energy of the beam.

PDD results show good agreement between data from EC measurements and MC simulations. Percentage difference does not exceed 7% but is important consider that future studies could include a new set of measurements with the extrapolation chamber confirming PDD profiles quantified here. Other plans, also may include MC simulations of beam modifiers, oblique beams and electron beams.

Appendix A

PENELOPE-PenEasy code

A complete description of the simulation package PENELOPE can be found in Salvat et al. (2011), besides about PenEasy main program was explained and is accessible to download in the web page of INTE (Institut de Tècniques Energètiques) `http://inte.upc.edu/downloads`. This passage of the work pretends to show structure and documentation corresponding to main routines and subroutines used in the simulations. If user requires extensible information, read documentation is recommended.

A.1 Subroutine PenEasy

PenEasy is a free and open software. It is written in FORTRAN77 and its structure is shown in Figure A.1.

General description is as follows: Each cycle of the loop *history* performs the simulation of one primary particle and all its descendants (electromagnetic shower), each cycle of *particle* simulates a single photon, electron or positron and each cycle *interact* reproduces a single interaction, or the crossing of an interface if the distance to the intersection is shorten than the distance to the next interaction. The simulation of a particle ends she it leaves the material system or when its kinetic energy falls bellow some user-defined absorption energy which may depend on the material and particle type Badal (2008). Source configuration allows the generation of initial particles and their posterior changes. Tallies modules are the most important part to the user because with them, quantities of interest can be scored. Each one is presented below.

A.1.1 Source model

In this project PSF source model was employed, it reads the initial state of the particles to simulate from an external file (one for 6MV and other 15 MV). PSF is a plain text

```
call init; n=0                          ! Initialisation
history: do                             ! One history
  n = n+1                               ! Update history counter
  call CLEANS                           ! Clear stack
  call source                           ! Create primary particle
  particle: do                          ! One particle
    call SECPAR(left)                   ! Retrieve particle from stack
    if (left.eq.0) exit particle        ! Stack was empty
    call START                          ! Reset transport mechanics
    interact: do                        ! One interaction/intersection
      call JUMP(dsmax(mat),ds)          ! Distance to interaction
      call STEP(ds,dsef,ncross)         ! Geometry check
      if (ncross.ne.0) then             ! Interface crossed
        if (mat.eq.0) exit interact     ! Particle is gone
        call START                      ! Reset transport mechanics
        cycle interact                  ! Start over
      endif
      call KNOCK(de,icol)               ! Simulate an interaction
      if (e.lt.eabs(kpar,mat)) exit interact   ! Absorbed
    enddo interact
  enddo particle
  if (endsim(n)) exit history           ! Check end-of-simulation
enddo history
call report
```

FIGURE A.1: Basic structure of the Fortran version of PenEasy. Tallies and auxiliary subroutines are missing Badal (2008).

file that contains information about beam energy, field size, angle of beam incidence and SSD. Module Source Phase Space File is shown in Figure A.2.

```
[SECTION SOURCE PHASE SPACE FILE v.2009-06-15]
 ON                                 STATUS (ON or OFF)
 0                                  PSF FORMAT (0=STANDARD penEasy ASCII; 1=IAEA BINARY)
 output.psf                         PSF FILENAME, REMOVE EXTENSION IF PSF FORMAT=1
 1                                  SPLITTING FACTOR
 0.0 180  0.0                       EULER ANGLES [Rz,Ry,Rz](deg) TO ROTATE POSITION AND DIRECTION
 0.0 0.0  0.0                       CARTESIAN COMPONENTS [DX,DY,DZ](cm) OF POSITION SHIFT
 1                                  VALIDATE BEFORE SIMULATION (1=YES, MAY TAKE A WHILE; 0=NO)
 0.000e0                            MAX PSF ENERGY (eV) (UNUSED IF VALIDATE=1; ADD 1023 keV FOR e+)
[END OF SPSF SECTION]
```

FIGURE A.2: Code Source Phase Space File

A.1.2 PENGEOM+PENVEOX section

User defines geometry used in the simulation with this module. It can be: quadrics, voxels or a mixture between both. Our phantom is a cube build from quadric surfaces using *PENGEOM* (geometry package of PENELOPE), the code is alike below:

```
 SURFACE ( 10) Plane Z=+100.0
INDICES=( 0, 0, 0, 1, 0)
Z-SHIFT=(+100.0000000000000E+00, 0)
0000000000000000000000000000000000000000000000000000000000000000
SURFACE ( 11) Plane Z=+100.1
INDICES=( 0, 0, 0, 1, 0)
```

```
Z-SHIFT=(+100.1000000000000E+00, 0)
00000000000000000000000000000000000000000000000000000000000000000000
SURFACE ( 12) Plane Z=+104.0
INDICES=( 0, 0, 0, 1, 0)
Z-SHIFT=(+104.0000000000000E+00, 0)
00000000000000000000000000000000000000000000000000000000000000000000
SURFACE ( 13) Plane Z=+110.0
INDICES=( 0, 0, 0, 1, 0)
Z-SHIFT=(+110.0000000000000E+00, 0)
00000000000000000000000000000000000000000000000000000000000000000000
SURFACE ( 14) Plane Z=+120.0
INDICES=( 0, 0, 0, 1, 0)
Z-SHIFT=(+120.0000000000000E+00, 0)
00000000000000000000000000000000000000000000000000000000000000000000
SURFACE ( 15) Plane Z=+99.9
INDICES=( 0, 0, 0, 1, 0)
Z-SHIFT=(+99.90000000000000E+00, 0)
00000000000000000000000000000000000000000000000000000000000000000000
SURFACE ( 16) Plane Z=+120.1
INDICES=( 0, 0, 0, 1, 0)
Z-SHIFT=(+120.1000000000000E+00, 0)
00000000000000000000000000000000000000000000000000000000000000000000
SURFACE ( 17) Plane X=-15.0
INDICES=( 0, 0, 0, 0, 0)
AX=(+1.000000000000000E+00, 0)
A0=(+15.00000000000000E+00, 0)
00000000000000000000000000000000000000000000000000000000000000000000
SURFACE ( 18) Plane X=+15.0
INDICES=( 0, 0, 0, 0, 0)
AX=(+1.000000000000000E+00, 0)
A0=(-15.00000000000000E+00, 0)
00000000000000000000000000000000000000000000000000000000000000000000
SURFACE ( 19) Plane Y=-15.0
INDICES=( 0, 0, 0, 0, 0)
AY=(+1.000000000000000E+00, 0)
A0=(+15.00000000000000E+00, 0)
00000000000000000000000000000000000000000000000000000000000000000000
SURFACE ( 20) Plane Y=+15.0
INDICES=( 0, 0, 0, 0, 0)
AY=(+1.000000000000000E+00, 0)
A0=(-15.00000000000000E+00, 0)
```

```
0000000000000000000000000000000000000000000000000000000000000000
BODY ( 1) Box1
MATERIAL( 1)
SURFACE ( 10), SIDE POINTER=(+1)
SURFACE ( 11), SIDE POINTER=(-1)
SURFACE ( 17), SIDE POINTER=(+1)
SURFACE ( 18), SIDE POINTER=(-1)
SURFACE ( 19), SIDE POINTER=(+1)
SURFACE ( 20), SIDE POINTER=(-1)
0000000000000000000000000000000000000000000000000000000000000000
BODY ( 2) Box2
MATERIAL( 2)
SURFACE ( 11), SIDE POINTER=(+1)
SURFACE ( 12), SIDE POINTER=(-1)
SURFACE ( 17), SIDE POINTER=(+1)
SURFACE ( 18), SIDE POINTER=(-1)
SURFACE ( 19), SIDE POINTER=(+1)
SURFACE ( 20), SIDE POINTER=(-1)
0000000000000000000000000000000000000000000000000000000000000000
BODY ( 3) Box3
MATERIAL( 3)
SURFACE ( 12), SIDE POINTER=(+1)
SURFACE ( 13), SIDE POINTER=(-1)
SURFACE ( 17), SIDE POINTER=(+1)
SURFACE ( 18), SIDE POINTER=(-1)
SURFACE ( 19), SIDE POINTER=(+1)
SURFACE ( 20), SIDE POINTER=(-1)
0000000000000000000000000000000000000000000000000000000000000000
BODY ( 4) Box4
MATERIAL( 3)
SURFACE ( 13), SIDE POINTER=(+1)
SURFACE ( 14), SIDE POINTER=(-1)
SURFACE ( 17), SIDE POINTER=(+1)
SURFACE ( 18), SIDE POINTER=(-1)
SURFACE ( 19), SIDE POINTER=(+1)
SURFACE ( 20), SIDE POINTER=(-1)
0000000000000000000000000000000000000000000000000000000000000000
BODY ( 5) Box5
MATERIAL( 3)
SURFACE ( 15), SIDE POINTER=(+1)
SURFACE ( 16), SIDE POINTER=(-1)
```

```
SURFACE ( 17), SIDE POINTER=(+1)
SURFACE ( 18), SIDE POINTER=(-1)
SURFACE ( 19), SIDE POINTER=(+1)
SURFACE ( 20), SIDE POINTER=(-1)
BODY ( 1)
BODY ( 2)
BODY ( 3)
BODY ( 4)
0000000000000000000000000000000000000000000000000000000000000000
SURFACE ( 21) Plane Z=0.00
INDICES=( 0, 0, 0, 1, 0)
0000000000000000000000000000000000000000000000000000000000000000
SURFACE ( 22) Plane Z=+300.0
INDICES=( 0, 0, 0, 1, 0)
Z-SHIFT=(+300.0000000000000E+00, 0)
0000000000000000000000000000000000000000000000000000000000000000
SURFACE ( 23) Cone
INDICES=( 1, 1,-1, 0, 0)
X-SCALE=(+1.000000000000000E+00, 0)
Y-SCALE=(+1.000000000000000E+00, 0)
Z-SCALE=(+1.000000000000000E+00, 0)
0000000000000000000000000000000000000000000000000000000000000000
MODULE ( 6) Volume inside the pair of planes and the cone
MATERIAL( 4)
SURFACE ( 21), SIDE POINTER=(+1)
SURFACE ( 22), SIDE POINTER=(-1)
SURFACE ( 23), SIDE POINTER=(-1)
BODY ( 5)
```

A.1.3 PENELOPE section

Material's files should be placed in this module (See Figure A.3). For a certain material, transport parameters could be set although if the user left those spaces in blank, program has a default values.

A.1.4 Tally Spatial Dose Distribution

Absorbed dose per simulated history is scored by this tally (See Figure A.4). Intervals and bins defined for x, y, and z axis were employed to quantify dose, definition allows

```
[SECTION PENELOPE v.2009-10-01]
 MAT# FILE___(max 20 char)     EABS(e-)  EABS(ph)  EABS(e+)  C1    C2    WCC      WCR      DSMAX
  1   plasticwater.mat         100.0e3   10.00e3   100.0e3   0.1   0.1   100.0e3  10.00e3  0.002e-3
  2   plasticwater.mat         100.0e3   10.00e3   100.0e3   0.1   0.1   100.0e3  10.00e3  0.01e0
  3   plasticwater.mat         100.0e3   10.00e3   100.0e3   0.1   0.1   100.0e3  10.00e3  0.01e0
  4   aircone.mat              100.0e3   10.00e3   100.0e3   0.1   0.1   100.0e3  10.00e3  0.01e0
  0 (SET MAT=0 TO END LIST)
[END OF PEN SECTION]
```

FIGURE A.3: Section PENELOPE inside the Main program

the scoring of a 3D spatial dose distribution in homogeneous regions. The relative uncertainty requested also is defined by this tally, user must take into account this value because it is used as a criterion to decide when to stop the simulation.

```
[SECTION TALLY SPATIAL DOSE DISTRIB v.2009-06-15]
 ON                                STATUS (ON or OFF)
 -2.0   2.0     1                  XMIN,XMAX(cm),NXBIN (0 for DX=infty)
 -2.0   2.0     1                  YMIN,YMAX(cm),NYBIN (0 for DY=infty)
 100    100.1   50                 ZMIN,ZMAX(cm),NZBIN (0 for DZ=infty)
 1                                 PRINT COORDINATES IN REPORT (1=YES,0=NO)
 3.0                               RELATIVE UNCERTAINTY (%) REQUESTED
[END OF SDD SECTION]
```

FIGURE A.4: Tally Spatial Dose Distribution to quantify absorbed dose within the first mm.

Tally Spatial Dose Distribution may be replicated by the user. This tally was used four times in the main program of this work Figure A.5, each one corresponds to one region of interest in our phantom.

A.1.5 Interaction forcing section

This module manages the variance reduction technique of interaction forcing. Module definition can be different according to the particles and interaction mechanisms for which forcing will be applied. See Figure A.6.

A.1.6 Particle splitting section

This module manages the variance reduction technique of particle splitting. User may specify: splitting mode, splitting factor and minimum value of statistical weight above method is applied. See Figure A.7.

```
[SECTION TALLY SPATIAL DOSE DISTRIB2 v.2009-06-15]
 ON                                  STATUS (ON or OFF)
 -2.0   2.0   1                       XMIN,XMAX(cm),NXBIN (0 for DX=infty)
 -2.0   2.0   1                       YMIN,YMAX(cm),NYBIN (0 for DY=infty)
 100.1  104   40                      ZMIN,ZMAX(cm),NZBIN (0 for DZ=infty)
 1                                   PRINT COORDINATES IN REPORT (1=YES,0=NO)
 3.0                                 RELATIVE UNCERTAINTY (%) REQUESTED
[END OF SDD2 SECTION]

[SECTION TALLY SPATIAL DOSE DISTRIB3 v.2009-06-15]
 ON                                  STATUS (ON or OFF)
 -2.0   2.0     1                   XMIN,XMAX(cm),NXBIN (0 for DX=infty)
 -2.0   2.0     1                   YMIN,YMAX(cm),NYBIN (0 for DY=infty)
 104    110     6                   ZMIN,ZMAX(cm),NZBIN (0 for DZ=infty)
 1                                   PRINT COORDINATES IN REPORT (1=YES,0=NO)
 3.0                                 RELATIVE UNCERTAINTY (%) REQUESTED
[END OF SDD3 SECTION]

[SECTION TALLY SPATIAL DOSE DISTRIB4 v.2009-06-15]
 ON                                  STATUS (ON or OFF)
 -2.0  2.0     1                    XMIN,XMAX(cm),NXBIN (0 for DX=infty)
 -2.0  2.0     1                    YMIN,YMAX(cm),NYBIN (0 for DY=infty)
 110   120    10                    ZMIN,ZMAX(cm),NZBIN (0 for DZ=infty)
 1                                   PRINT COORDINATES IN REPORT (1=YES,0=NO)
 3.0                                 RELATIVE UNCERTAINTY (%) REQUESTED
[END OF SDD4 SECTION]
```

FIGURE A.5: Replicated tallies Spatial Dose Distribution to quantify absorbed dose.

```
[SECTION INTERACTION FORCING v.2009-06-15]
 ON                                  STATUS (ON or OFF)
 0.001                               DON'T APPLY BELOW THIS STATISTICAL WEIGHT
 MAT  KPAR  ICOL  FORCING  (SET MAT=0 TO END LIST)
 1    2     1     2.0
 1    2     2     2.0
 1    2     3     2.0
 1    2     4     2.0
 1    2     7     2.0
 1    2     8     2.0
 0    0     0     2.0
[END OF VRIF SECTION]
```

FIGURE A.6: Interaction forcing section apply to photons.

```
[SECTION SPLITTING v.2009-06-15]
 ON                              STATUS (ON or OFF)
 0.001                           WMIN, DO NOT SPLIT BELOW THIS WEIGHT
 1                               SPLITTING MATERIAL
 1                               SPLITTING MODE (1=SIMPLE; 2=ROTATIONAL; 3=XY)
 6                               SPLITTING FACTOR, IGNORED FOR MODE=3
 0.0  0.0  0.0                   EULER ANGLES [Rz,Ry,Rz](deg), IGNORED FOR MODE=1
 0.0  0.0  0.0                   SHIFT (cm), IGNORED FOR MODE=1
 +                               SIGN OF W ('+', '-' OR '0'=BOTH), IGNORED FOR MODE=1
 0.0  360.0                      AZIMUTHAL INTERVAL PHI0 AND DeltaPHI (deg), ONLY IF MODE=2
[END OF VRS SECTION]
```

FIGURE A.7: Particle splitting, mode: Simple, Splitting factor: 6.0.

Appendix B

Regression models for the determination of the absorbed dose with extrapolation chamber

Empirical part of this project involves measurements with an extrapolation chamber. It has two flat parallel electrodes of variable separation; the input electrode is fixed in relation to the collector electrode of constant area. Determination of absorbed dose needs to estimate the extrapolation curve slope using a linear regression model on plots corresponding to separation distance against collected charge.

The analysis , in which absorbed dose should be determined is the same for each depth; taking into account three different distances for plate separation and their related mean charge value from measurements in both positive and negative bias voltage. Numerical results and linear models are presented above.

B.1 Results 6MV photon beam

B.1.1 Depth $z = 0.0\ mm$

Table B.1 indicates the measurements used to generate linear regression curve. Figure B.1 is the plot of this data and equation of the straight line can be read.

distance (mm)	Q (pC)
0.5	306.25
1,5	691.38
2.0	911.33

TABLE B.1: Results for 6MV photons $z = 0.0\ mm$.

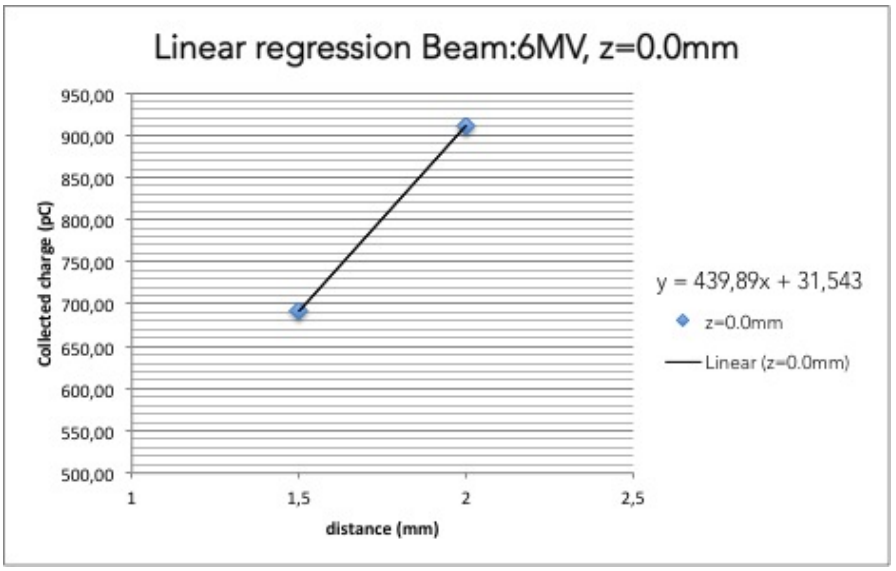

FIGURE B.1: Linear regression curve for 6MV photons, $z = 0.0\ mm$.

B.1.2 Depth $z = 1.0\ mm$

Table B.2 indicates the measurements used to generate linear regression curve. Figure B.2 is the plot of this data and equation of the straight line can be read.

distance (mm)	Q (pC)
0.5	1062.8
1.5	2129.0
2.0	2639.0

TABLE B.2: Results for 6MV photons $z = 1.0\ mm$.

B.1.3 Depth $z = 2.0\ mm$

Table B.3 indicates the measurements used to generate linear regression curve. Figure B.3 is the plot of this data and equation of the straight line can be read.

distance (mm)	Q (pC)
0.5	1445.3
1.5	2881.8
2.0	3585.3

TABLE B.3: Results for 6MV photons $z = 2.0\ mm$.

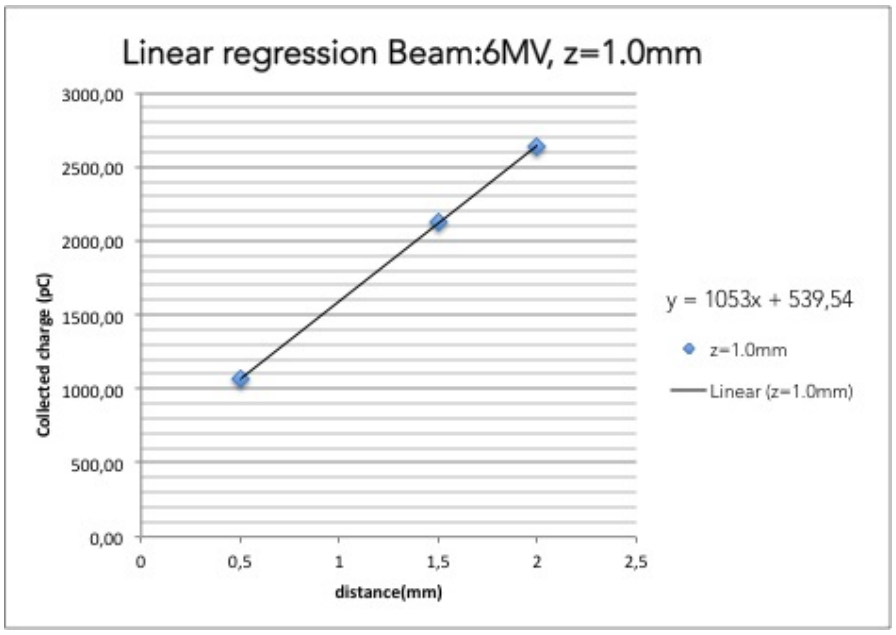

FIGURE B.2: Linear regression curve for 6MV photons, $z = 1.0\ mm$.

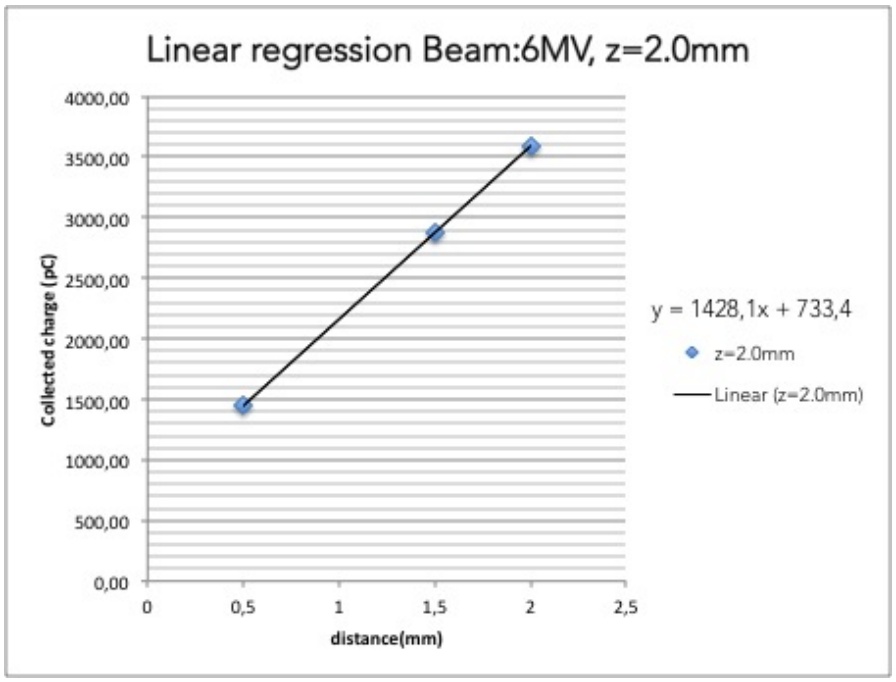

FIGURE B.3: Linear regression curve for 6MV photons, $z = 2.0\ mm$.

B.1.4 Depth $z = 4.0\ mm$

Table B.4 indicates the measurements used to generate linear regression curve. Figure B.4 is the plot of this data and equation of the straight line can be read.

distance (mm)	Q (pC)
0.5	1872.2
1.5	3704.5
2.0	4612.3

TABLE B.4: Results for 6MV photons $z = 4.0\ mm$.

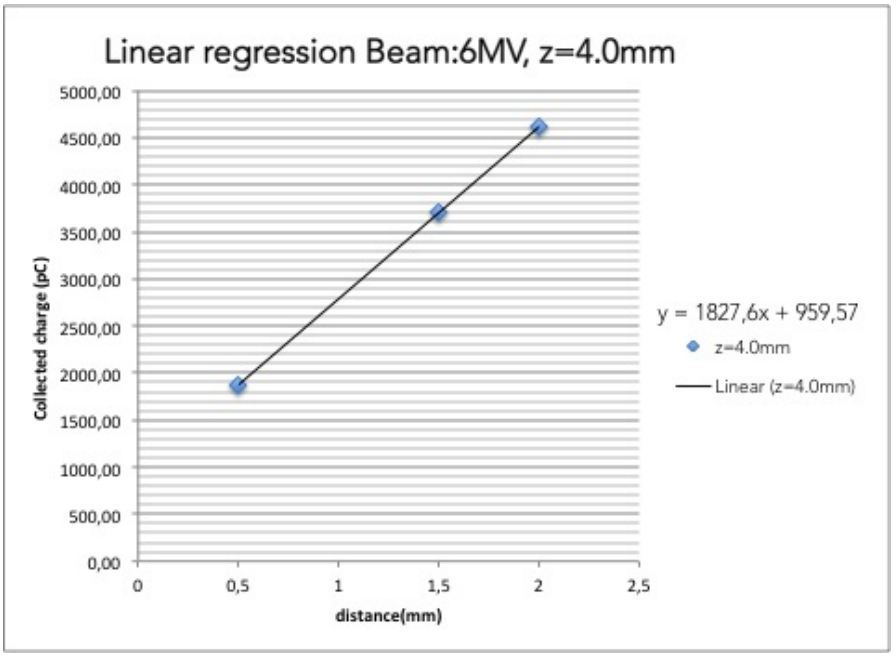

FIGURE B.4: Linear regression curve for 6MV photons, $z = 4.0\ mm$.

B.1.5 Depth $z = 5.0\ mm$

Table B.5 indicates the measurements used to generate linear regression curve. Figure B.5 is the plot of this data and equation of the straight line can be read.

distance (mm)	Q (pC)
0.5	1872.0
1.5	3074.5
2.0	4612.3

TABLE B.5: Results for 6MV photons $z = 5.0\ mm$.

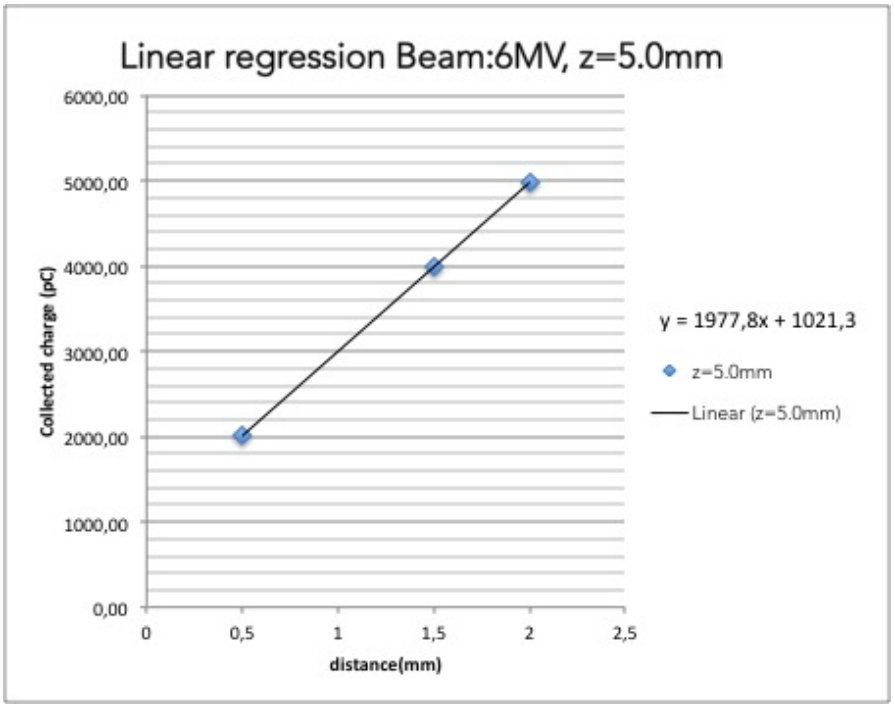

FIGURE B.5: Linear regression curve for 6MV photons, $z = 5.0\ mm$.

B.1.6 Depth $z = 7.0\ mm$

Table B.6 indicates the measurements used to generate linear regression curve. Figure B.6 is the plot of this data and equation of the straight line can be read.

distance (mm)	Q (pC)
0.5	2209.0
1.5	4320.3
2.0	5345.3

TABLE B.6: Results for 6MV photons $z = 2.0\ mm$.

B.1.7 Depth $z = 10\ mm$

Table B.7 indicates the measurements used to generate linear regression curve. Figure B.7 is the plot of this data and equation of the straight line can be read.

distance (mm)	Q (pC)
0.5	2312.8
1.5	4541.5
2.0	5595.2

TABLE B.7: Results for 6MV photons $z = 10\ mm$.

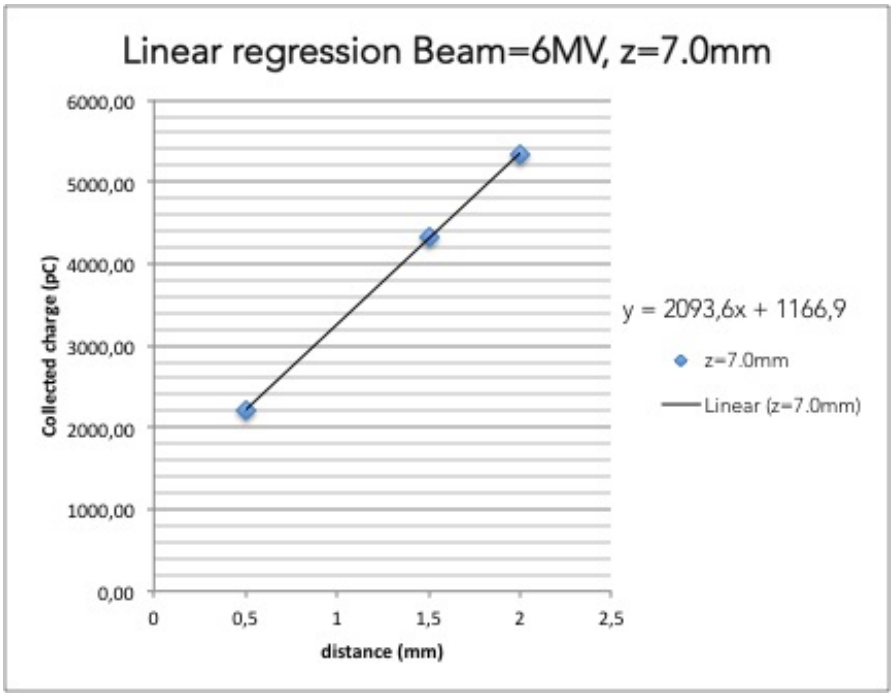

FIGURE B.6: Linear regression curve for 6MV photons, $z = 7.0\ mm$.

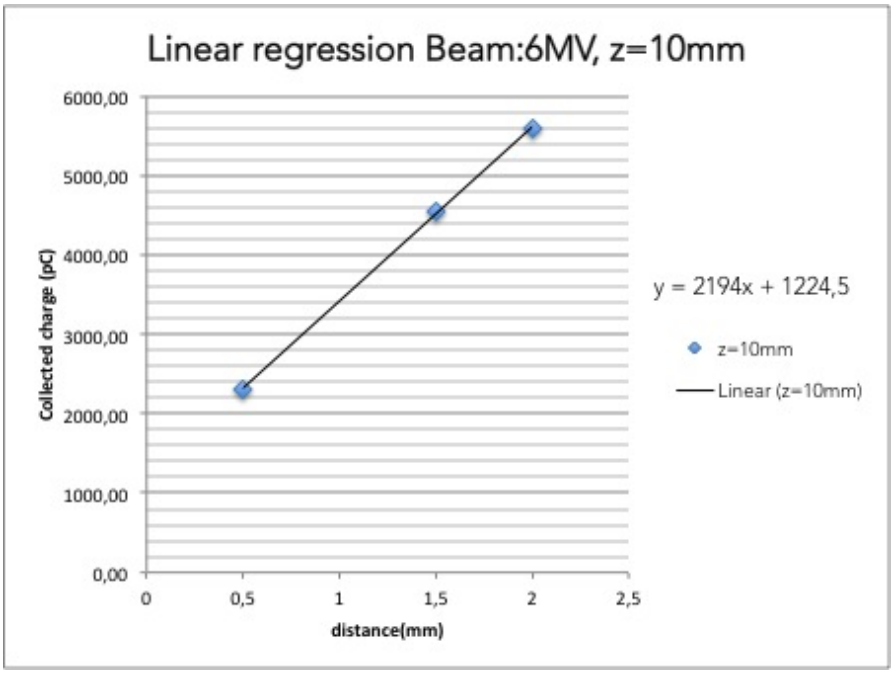

FIGURE B.7: Linear regression curve for 6MV photons, $z = 10\ mm$.

B.1.8 Depth $z = 15\ mm$

Table B.8 indicates the measurements used to generate linear regression curve. Figure B.8 is the plot of this data and equation of the straight line can be read.

distance (mm)	Q (pC)
0.5	2312.8
1.5	4541.5
2.0	5595.2

TABLE B.8: Results for 6MV photons $z = 15\ mm$.

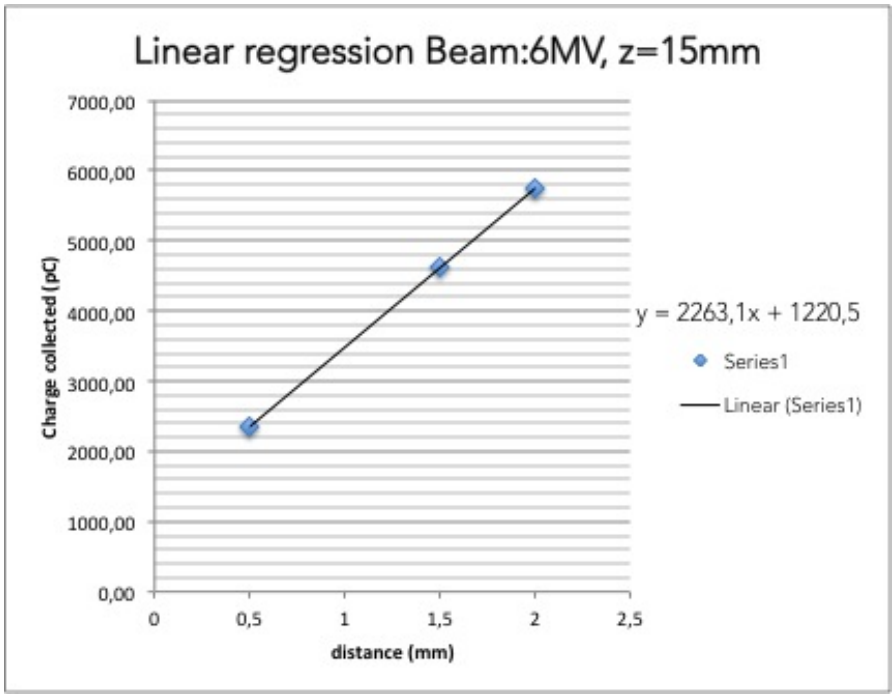

FIGURE B.8: Linear regression curve for 6MV photons, $z = 15\ mm$.

B.2 Results 15MV photon beam

B.2.1 Depth $z = 0.0\ mm$

Table B.9 indicates the measurements used to generate linear regression curve. Figure B.9 is the plot of this data and equation of the straight line can be read.

B.2.2 Depth $z = 1.0\ mm$

Table B.10 indicates the measurements used to generate linear regression curve. Figure B.10 is the plot of this data and equation of the straight line can be read.

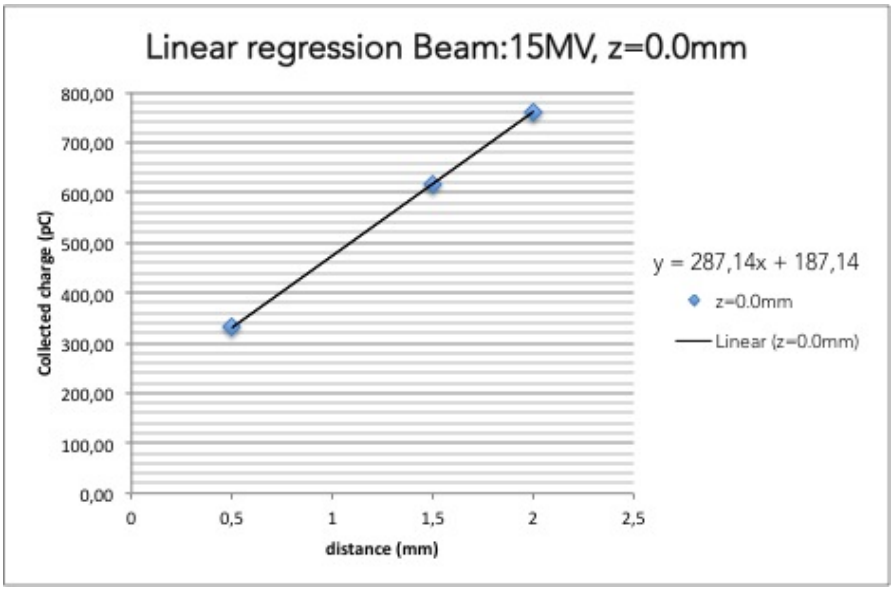

FIGURE B.9: Linear regression curve for 15MV photons, $z = 0.0\ mm$.

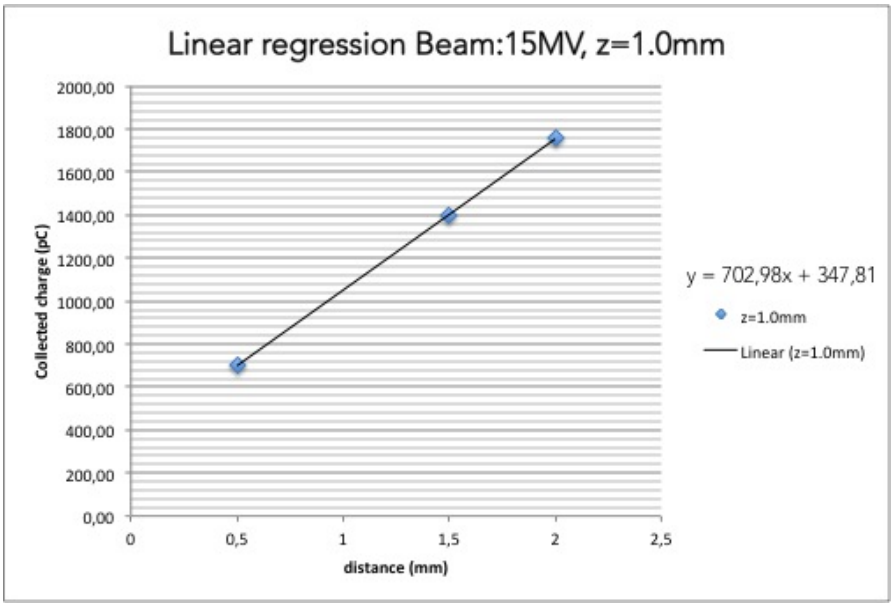

FIGURE B.10: Linear regression curve for 15MV photons, $z = 1.0\ mm$.

distance (mm)	Q (pC)
0.5	330.6
1.5	618.3
2.0	761.2

TABLE B.9: Results for 15MV photons $z = 0.0\ mm$.

distance (mm)	Q (pC)
0.5	700.3
1.5	1399.2
2.0	1755.8

TABLE B.10: Results for 15MV photons $z = 1.0\ mm$.

B.2.3 Depth $z = 2.0\ mm$

Table B.11 indicates the measurements used to generate linear regression curve. Figure B.11 is the plot of this data and equation of the straight line can be read.

distance (mm)	Q (pC)
0.5	836.7
1.5	1957.3
2.0	2445.7

TABLE B.11: Results for 15MV photons $z = 2.0\ mm$.

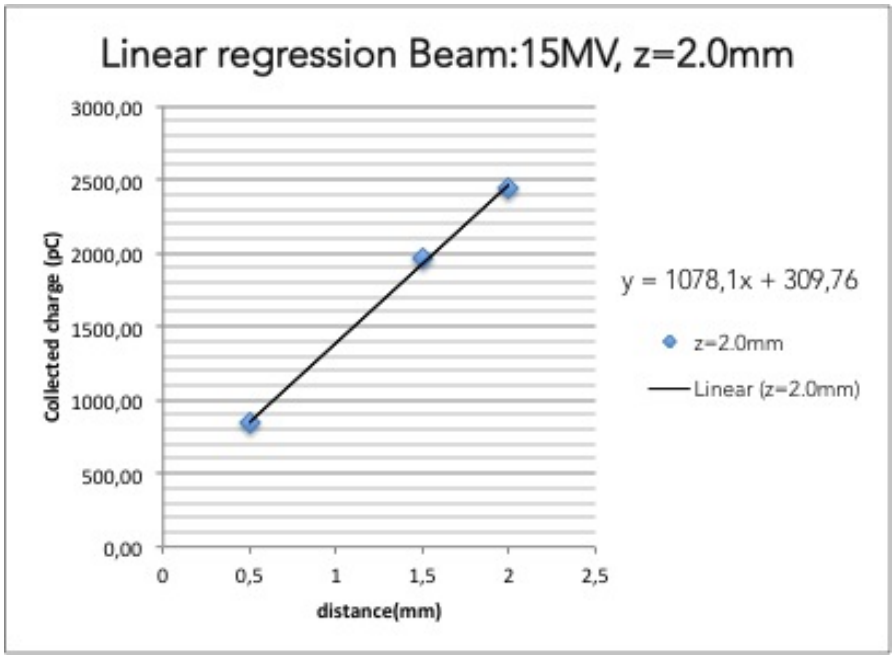

FIGURE B.11: Linear regression curve for 15MV photons, $z = 2.0\ mm$.

B.2.4 Depth $z = 4.0\ mm$

Table B.12 indicates the measurements used to generate linear regression curve. Figure B.12 is the plot of this data and equation of the straight line can be read.

distance (mm)	Q (pC)
0.5	1381.7
1.5	2763.2
2.0	3416.2

TABLE B.12: Results for 15MV photons $z = 4.0\ mm$.

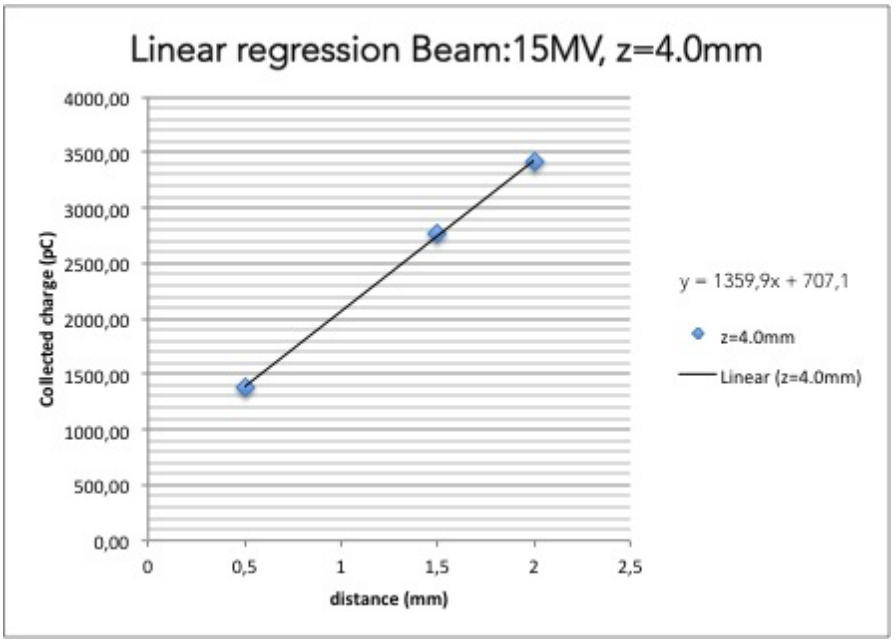

FIGURE B.12: Linear regression curve for 15MV photons, $z = 4.0\ mm$.

B.2.5 Depth $z = 5.0\ mm$

Table B.13 indicates the measurements used to generate linear regression curve. Figure B.13 is the plot of this data and equation of the straight line can be read.

distance (mm)	Q (pC)
0.5	1539.8
1.5	3045.3
2.0	3797.5

TABLE B.13: Results for 15MV photons $z = 5.0\ mm$.

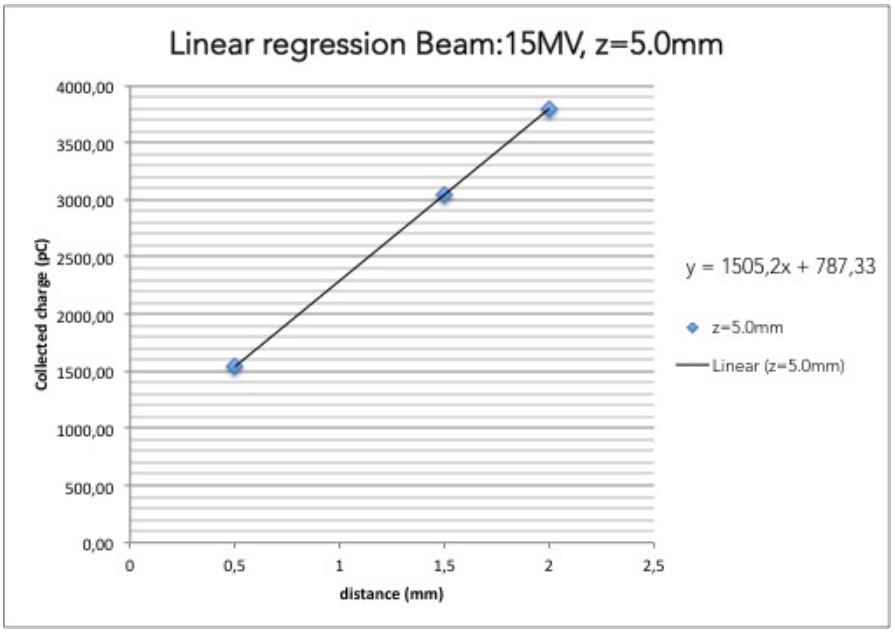

FIGURE B.13: Linear regression curve for 15MV photons, $z = 5.0\ mm$.

B.2.6 Depth $z = 7.0\ mm$

Table B.14 indicates the measurements used to generate linear regression curve. Figure B.14 is the plot of this data and equation of the straight line can be read.

distance (mm)	Q (pC)
0.5	1796.3
1.5	3503.6
2.0	4332.5

TABLE B.14: Results for 15MV photons $z = 7.0\ mm$.

B.2.7 Depth $z = 10\ mm$

Table B.15 indicates the measurements used to generate linear regression curve. Figure B.15 is the plot of this data and equation of the straight line can be read.

distance (mm)	Q (pC)
0.5	2007.0
1.5	3934.3
2.0	4865.9

TABLE B.15: Results for 15MV photons $z = 10\ mm$.

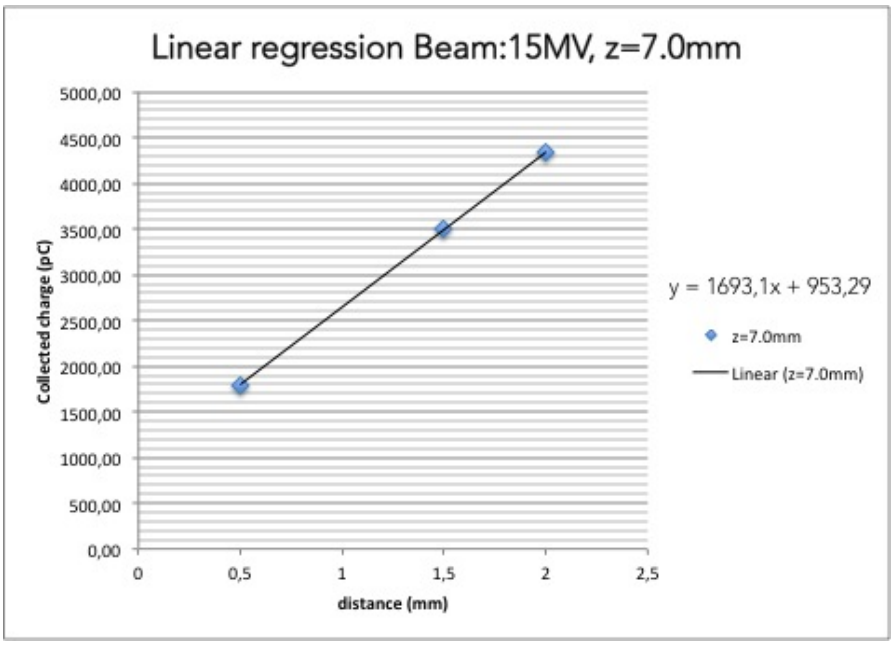

FIGURE B.14: Linear regression curve for 15MV photons, $z = 7.0\ mm$.

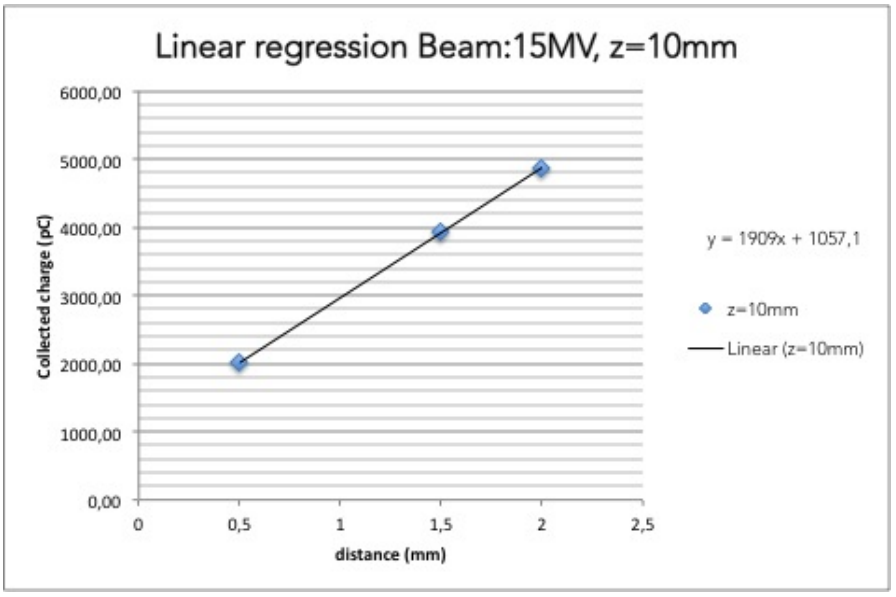

FIGURE B.15: Linear regression curve for 15MV photons, $z = 10\ mm$.

B.2.8 Depth $z = 15\ mm$

Table B.16 indicates the measurements used to generate linear regression curve. Figure B.16 is the plot of this data and equation of the straight line can be read.

distance (mm)	Q (pC)
0.5	2222.7
1.5	4356.3
2.0	5408.3

TABLE B.16: Results for 15MV photons $z = 15\ mm$.

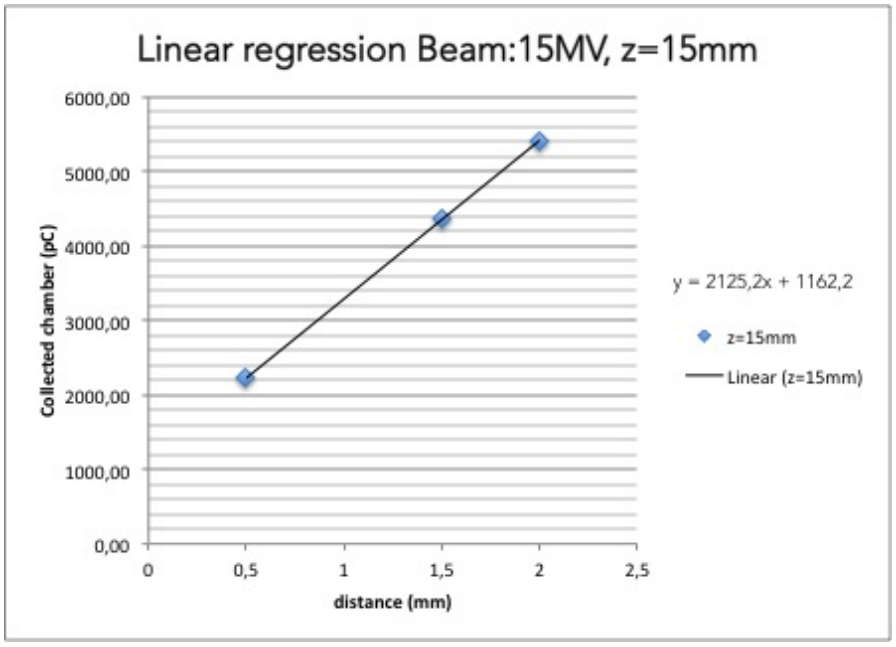

FIGURE B.16: Linear regression curve for 15MV photons, $z = 15\ mm$.

B.2.9 Depth $z = 30\ mm$

Table B.17 indicates the measurements used to generate linear regression curve. Figure B.17 is the plot of this data and equation of the straight line can be read.

distance (mm)	Q (pC)
0.5	2359.5
1.5	4645.8
2.0	5511.8

TABLE B.17: Results for 15MV photons $z = 30\ mm$.

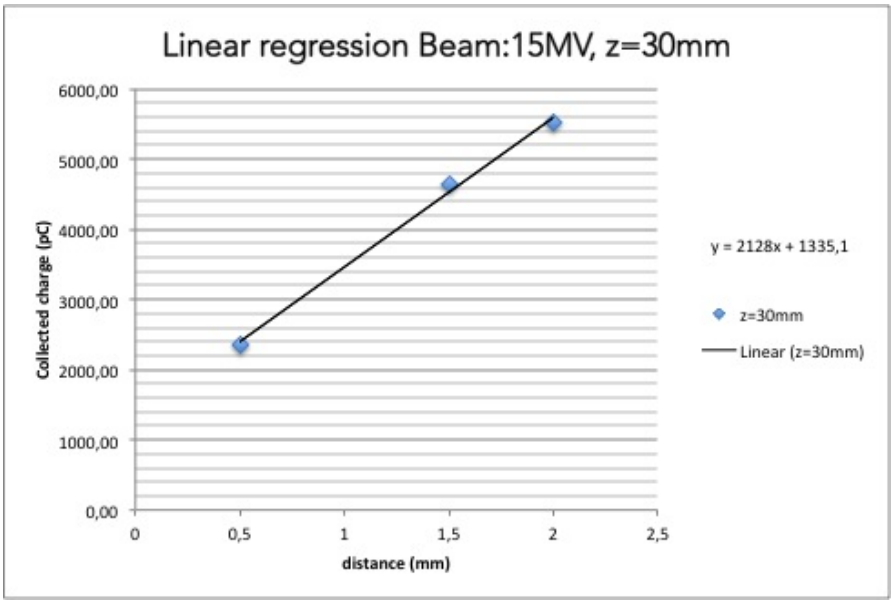

FIGURE B.17: Linear regression curve for 15MV photons, $z = 30\ mm$.

Measuring these chosen points for all cases, error under 2% has been assured in each linear regression, respect to the reported real zero for the extrapolation chamber was used in this work. Finally extrapolation curve slopes was calculated from the data presented in the appendix then PDD can be calculated and related with direct measurements obtained at the experiment.

Acknowledgements

A Dios y a esas personas que pone en mi camino para que la vida se haga fácil de llevar y los sueños posibles de cumplir (pido de ante mano disculpas porque aunque muchos no están nombrados fueron parte del proceso y los llevo en el corazón)... a cada uno de ellos infinitas GRACIAS!

Momita gracias por la vida, por el amor, por ser mi soporte, por estar incondicionalmente para mí, junto a Nata y Karentuty son mi pequeña pero maravillosa fortaleza, su apoyo y compañía son vitales en este camino y hacen de mí una mejor persona. A ellas y los demás miembros de mi familia gracias por la confianza depositada y les dedico esta nueva meta superada.

Personas que conoces y se vuelven incondicionales: Carlos bastaría con decir que eres mi hermano en toda regla: el del amor infinito, la confianza incondicional, el de los sueños planeados, cumplidos y por hacer; que importa la genética, la presencia o la ausencia eres parte de mi familia y eso lo dice todo: gracias. Davide y Olgauss mis incondicionales porque a pesar de los km y fronteras que nos separan son los mejores amigos y los siento más cerca que nunca; gracias por abrirme espacio en su vida y escribir juntos una historia. Juan Francisco y Felipe los admiro infinito, los quiero, gracias por enseñarme tantas cosas a nivel personal y académico; en cualquier lugar del mundo sé que compartir momentos con ustedes será de las mejores cosas que me pasen en la vida. Juan David, Daniel, Lauris M., Juli, y Lauris A. los quiero un montón con ustedes sé que la amistad no se mide con la frecuencia sino con el corazón. No menos importante, Diana, mi mamá en Barcelona, miles y miles de gracias porque fuiste mi apoyo, mi familia, mi amiga, mi confidente en esta aventura, esta Ingrid dos años después no sería la misma si la vida no te hubiera puesto en mi camino.

De manera especial, quiero darle las gracias a mi tutora Dra. María Amor Duch, por proponerme este proyecto, por su soporte científico, por los conocimientos adquiridos, su paciencia y gran apoyo durante esta etapa. Fue para mi un placer haber trabajado en un tema que me apasiona y en el cual quiero desarrollar mi carrera como investigadora. Además agradezco al INTE (Instituto de Técnicas Energéticas) de la UPC donde tuve la oportunidad de trabajar, en especial, al grupo dedicado a Monte Carlo y en él a Marta Bueno por todo su soporte en cuanto a Penelope, PenEasy y PSFs se refiere.

Para concluir, doy las gracias a Colfuturo sin su programa no hubiera sido posible cumplir el objetivo de hacer mi maestría fuera de Colombia y tener hoy este proyecto en mis manos; tuve la oportunidad de trabajar en lo que me gusta, conocer lugares y personas maravillosas, aprender, y sobretodo pude y podré compartir y seguir cultivando mis sueños. Agradezco igualmente la ayuda económica adjudicada por la cátedra Argos para la realización y consecución de este proyecto de fin de Máster.

Bibliography

Apipunyasopon, L., Srisatit, S., and Phaisangittisakul, N. (2013). An investigation of the depth dose in the build-up region, and surface dose for a 6-MV therapeutic photon beam: Monte Carlo simulation and measurements. *Journal of radiation research*, 54(2):374–82.

Badal, A. (2008). *Development of advanced geometric models and acceleration techniques for Monte Carlo simulation in Medical Physics*. PhD thesis, Universitat de Barcelona-Universidad Politécnica de Cataluña.

Bielajew, A. F. and Carlo, M. M. (1991). Chapter 1 : History of Monte Carlo. Technical report, University of Michigan, Michigan.

Buston, M., Cheung, T., and Yu, P. (2006). Skin Dose Delivered in Megavoltage External Beam Therapeutic Radiology. *Austral-Asian Journal of Cancer*, 5(2):101–104.

GmbH, P. F. (2012). Böhm Extrapolation Chamber.

Hernández, F. (2012). *Posta a punt d'un sistema per la determinaciò de la dosi en pell durant tractaments de radioterápia.* Projecte final de máster, Universitat de Barcelona- Universitat Politècnica de Catalunya.

Ishmael Parsai, E., Shvydka, D., Pearson, D., Gopalakrishnan, M., and Feldmeier, J. J. (2008). Surface and build-up region dose analysis for clinical radiotherapy photon beams. *Applied radiation and isotopes : including data, instrumentation and methods for use in agriculture, industry and medicine*, 66(10):1438–42.

Jayaraman, S. (2004). *Clinical Radiotherapy Physics*. Springer, Heidelberg, Germany.

Kron, T., Elliot, A., Wong, T., Showell, G., Clubb, B., and Metcalfe, P. (1993). Xray surface dose measurements using TLD extrapolation. *Journal of Medical Physics*, 20(3):9.

Kry, S. F., Smith, S. a., Weathers, R., and Stovall, M. (2012). Skin dose during radiotherapy: a summary and general estimation technique. *Journal of applied clinical medical physics American College of Medical Physics*, 13(3):3734.

Lee, N., Chuang, C., Quivey, J. M., Phillips, T. L., Akazawa, P., Verhey, L. J., and Xia, P. (2002). Skin toxicity due to intensity-modulated radiotherapy for head-and-neck carcinoma. *International journal of radiation oncology, biology, physics*, 53(3):630–7.

Lin, J.-P., Chu, T.-C., Lin, S.-Y., and Liu, M.-T. (2001). Skin dose measurement by using ultra-thin TLDs. *Applied Radiation and Isotopes*, 55(3):383–391.

Mayles, P., Nahum, A., and Rosenwald, J. (2007). *Handbook of Radiotherapy Physics-Theory and Practice*. Taylor & Francis, United States of America.

Metcalfe, P., Kron, T., and Hoban, P. (2007). *The Physics of Radiotherapy X-Rays and Electrons.* Medical Physics Publishing, Vernon, Madison, 2 edition.

Nilsson, B. and Sorcini, B. (1989). Surface dose measurements in clinical photon beams. *Acta oncologica (Stockholm, Sweden)*, 28(4):537–42.

Panettieri, V., Barsoum, P., Westermark, M., Brualla, L., and Lax, I. (2009). AAA and PBC calculation accuracy in the surface build-up region in tangential beam treatments. Phantom and breast case study with the Monte Carlo code PENELOPE. *Radiotherapy and oncology : journal of the European Society for Therapeutic Radiology and Oncology*, 93(1):94–101.

Podgorsak, E. B. and Kainz, K. (2005). *Radiation Oncology Physics: A Handbook for Teachers and Students*, volume 33. International Atomic Energy Agency, Vienna, Austria.

Rawlinson, J., Arlen, D., and Newcombe, D. (1992). Design of parallel plate ion chambers for buildup measurements in megavoltage photon beams. *Medical Physics*, 19(3):641–648.

Rikner, G. and Grusell, E. (1987). Patient dose measurements in photon fields by means of silicon semiconductor detectors. *Medical Physics*, 14(5):870.

Salvat, F., Fernández-Varea, J., and Sempau, J. (2011). *PENELOPE-2011: A code system for Monte Carlo simulation of electron and photon transport*. Nuclear Energy Agency, Barcelona, Spain.

Thomas, S. and Palmer, N. (1989). The use of carbon-loaded thermoluminescent dosimeters for the measurement of surface doses in megavoltage x-ray beams. *Medical Physics*, 16(6):902–904.

Wells, M. and Macbride, S. (2003). Radiation skin reactions. In *Supportive care in radiotherapy*, chapter 8, page 418. Churchill Livingstone, UK.

Yadav, G., Yadav, R., and Kumar, A. (2010). Effect of various physical parameters on surface and build-up dose for 15-MV X-rays. *Journal of Medical Physics*, 35(4):202–206.

Zankowski, C. E. and Podgorsak, E. B. (1997). Calibration of photon and electron beams with an extrapolation chamber. *Medical physics*, 24(4):497–503.

UNIVERSITAT POLITÈCNICA DE CATALUNYA

UNIVERSITAT DE BARCELONA

Projecte Final d'Estudis
MÀSTER EN ENGINYERIA BIOMÈDICA

Projecte Final d'Estudis presentat el dia de de 200 amb la següent Comissió Avaluadora:

Dr. President

Dr. Vocal 1

Dr. Vocal 2

Dr. Secretari

Amb la qualificació de:

UNIVERSITAT POLITÈCNICA
DE CATALUNYA

UNIVERSITAT DE BARCELONA